SSD-TDR 64-90

601323

2 of 3

71-p $2.00

A Study of Artificial Dielectrics

15 MAY 1964

Prepared by K. E. GOLDEN
Plasma Research Laboratory

Prepared for BALLISTIC SYSTEMS AND SPACE SYSTEMS DIVISIONS
AIR FORCE SYSTEMS COMMAND
El Segundo, California

LABORATORY OPERATIONS • AEROSPACE CORPORATION
CONTRACT NO. AF 04(695)-269

SSD-TDR-64-90

Report No.
TDR-269(4280-10)-4

A STUDY OF ARTIFICIAL DIELECTRICS

Prepared by

Kurt E. Golden
Plasma Research Laboratory

AEROSPACE CORPORATION
El Segundo, California

Contract No. AF 04(695)-269

15 May 1964

Prepared for

BALLISTIC SYSTEMS AND SPACE SYSTEMS DIVISIONS
UNITED STATES AIR FORCE COMMAND
Inglewood, California

SSD-TDR-64-90

Report No.
TDR-269(4280-10)-4

A STUDY OF ARTIFICIAL DIELECTRICS

Prepared

K. E. Golden
Plasma Physics Department

Approved

R. H. Huddlestone, Head
Plasma Physics Department

R. X. Meyer, Director
Plasma Research Laboratory

This technical documentary report has been reviewed and is approved for publication and dissemination. The conclusions and finding contained herein do not necessarily represent an official Air Force position.

For Space Systems Division
Air Force Systems Command:

Kenneth R. Hughey
Captain, USAF

AEROSPACE CORPORATION
El Segundo, California

ABSTRACT

The simulation of a plasma sheath using an artificial dielectric is studied in this investigation and is applied to an antenna geometry which is similar to some configurations encountered in aerospace applications. The antenna configuration is equivalent to a horn in an infinite ground plane with an unbounded plasma layer in front of the horn. The plasma layer is simulated by a rodded medium, and the radiation patterns of the antenna system are studied experimentally at 9, 10, and 11 KMC.

The characteristics of a rodded medium are obtained both theoretically and experimentally. It is shown that a rodded medium not only simulates the isotropic characteristics of a plasma sheath but also the anisotropic characteristics of a plasma in an infinite steady magnetic field. If the rods are oriented in one direction, the equivalent tensor permittivity of the rodded medium is in the same form as the tensor permittivity of a cold plasma in a very strong magnetostatic field. The theoretical analysis is based on the geometrical symmetries of the medium and the transmission line approach to propagation in an artificial dielectric of periodically spaced conducting obstacles.

The anisotropic characteristics of a rodded medium are demonstrated in X-band waveguide measurements.

Two constructions of rodded media are utilized in the pattern measurements. The experimentally determined radiation patterns seem to have a secondary maximum associated with the properties of the plasma sheath. More energy is radiated in the off-axis region when the plasma sheath is present.

CONTENTS

FIGURES

FIGURES (Continued)

I. INTRODUCTION

The purpose of this investigation was to study plasma simulation using a rodded medium and to study the radiation patterns of an X-band horn antenna in the presence of a simulated plasma sheath. The plasma sheath is assumed to be under dense or operating above the plasma frequency. The antenna geometry is shown in Figure 1. Several authors[1,2,3,4] have studied this geometry or very similar geometries previously, but to obtain a clean experiment using a laboratory plasma is very difficult. Typically, the experimental and theoretical geometries are not the same. Usually the theoretical models are highly idealized and only approximate the actual experimental geometry because of the inherent difficulties in obtaining a solution to Maxwell's Equations for the actual geometry of interest. For example, the theoretical models pertaining to this study assume that the plasma sheath is unbounded, and the ground plane is infinite in extent, while the physical dimensions of the laboratory apparatus are finite in size. The glass walls which confine the gaseous discharge may also complicate the experimental geometry. The theoretical models neglect nonuniformities in the sheath which may be present in the actual laboratory experiment. In the final analysis the experimental measurements prove or disprove the validity of the theoretical model used to approximate the actual geometry under investigation.

Theoretical Models

Umura[2] obtained the expressions governing the far field radiation patterns of an infinitely long slot antenna in a ground plane which is covered with a plasma sheath. The analysis is based on Fourier Transform techniques and assumes two different aperture distributions. In the evaluation of the far field patterns the contributions of surface and complex waves are neglected. One of the distributions is equal to a constant electric field developed across the gap. The other distribution assumes that the electric field is parallel to the edge of the slit and has a co-sinusoidal distribution across the gap. The E plane and H plane radiation patterns of the horn geometry can be approximated

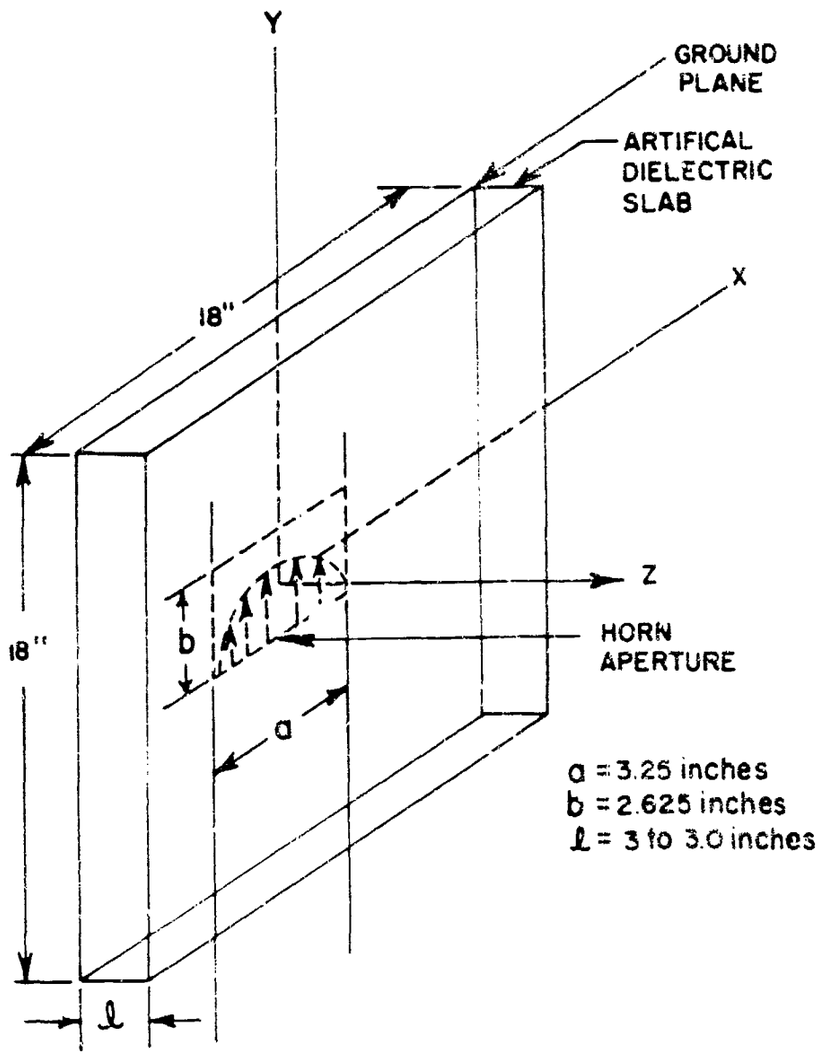

FIGURE 1 - Antenna geometry used in experimental study.

by the two equivalent slit problems[5] described above. Aside from the cylindrical or spherical wave terms of the far field radiation patterns, the algebraic expressions which relate the relative pattern changes of the horn and equivalent slit in the presence of the plasma are approximately equal and identical when the plasma layer is removed. The radiation from the slit, which has a constant electric field developed across the gap, is given by Equation (1) and is equal to the E plane pattern of the horn geometry.

$$P_\theta \propto \left[\frac{\sin\left(\frac{k_o b}{2} \sin\theta\right)}{\frac{k_o b}{2} \sin\theta} \right]^2 \left[\frac{1}{\cos^2(K_z \ell) + \frac{1}{n^4}\left(\frac{n^2 - \sin^2\theta}{\cos^2\theta}\right) \sin^2(K_z \ell)} \right] \quad (1)$$

Similarly, the patterns obtained from the slit, which are excited with the co-sinusoidal distribution, resemble the H plane patterns of the horn antenna and are expressed by Equation (2).

$$P_\phi \propto \left[\frac{\pi^2}{4} \cos\theta \, \frac{\cos\left(\frac{k_o a}{2} \sin\theta\right)}{\left(\frac{\pi}{2}\right)^2 - \left(\frac{k_o a}{2} \sin\theta\right)^2} \right]^2 \left[\frac{1}{\cos^2(K_z \ell) + \left(\frac{\cos^2\theta}{n^2 - \sin^2\theta}\right) \sin^2(K_z \ell)} \right] \quad (2)$$

The index of refraction of the plasma is given by

$$n^2 = 1 - \frac{\omega_p^2}{\omega^2} ,$$

where ω_p is the plasma frequency and ω is the wave frequency. The dimension of the aperture and the thickness of the plasma layer are equal to a, b, and ℓ respectively. The equivalent Z component of the wavenumber in the plasma is equal to

$$K_z = k_o \sqrt{n^2 - \sin^2\theta} .$$

Flock[3,4] studied the horn geometry from both a theoretical and experimental standpoint. The theoretical model assumes that the dominant pattern changes are caused by the currents induced in the plasma region directly in front of the horn and all other currents in the plasma are zero. The currents directly in front of the aperture are assumed to have a co-sinusoidal distribution in the X direction similar to the distribution of magnetic current in the aperture. The analysis neglects the effects produced by the currents which are induced in other regions of the plasma by the near fields of the horn. The theoretical calculations predict that the radiation from the equivalent source in the plasma will have a maximum at an angle θ_M given by

$$\cos \theta_M = n \ ,$$

when ω is greater than ω_p.
The gaseous discharge which he used in the experimental apparatus had dimensions of the order of an X-band standard gain horn which restricts the interpretation of the experimental results in terms of the unbounded plasma layer model.

Artificial Dielectrics

The radiation patterns described in this report have been studied experimentally using an artificial dielectric to simulate the properties of the plasma sheath. An artificial dielectric is used to alleviate some of the experimental difficulties of performing the measurements with a laboratory plasma. The artificial dielectric slab can be made large enough to approximate the conditions of an unbounded plasma layer. Also, the electromagnetic properties of an artificial dielectric are homogeneous and are characterized by an equivalent plasma frequency which can be determined theoretically within reasonable limits. The experimental measurements can be performed in a steady state condition and do not have to rely on the shot to shot reproducibility of a gaseous discharge. The main attribute of the artificial dielectric is the ease of controlling the experimental variables such as the size of the slab, the

equivalent plasma frequency or the thickness of the sheath.

Recently, it was observed[6] that the complex dielectric constant of a homogeneous isotropic plasma could be simulated by a rodded medium. The currents induced in the rods tend to simulate the oscillating inductive currents in a plasma thereby making the simulation possible. In general, the rods form a cubical lattice if the dielectric properties are to be isotropic for all polarizations.

Like a crystal lattice structure, an artificial dielectric can also exhibit anisotropic[7,8,9] behavior under certain conditions. In principle, it should therefore be possible to simulate the anisotropic behavior of a plasma[10] in an infinite magnetostatic field with a rodded medium. For these conditions the electrons in the plasma are confined to move along the magnetic lines of force. Anisotropic characteristics of a rod medium are observed when the rods are oriented in one or two directions. The induced currents are restricted to flow along certain preferred directions, namely along the rods. Therefore, the propagation characteristics of the rodded medium are a function of the polarization of the electric field making the medium anisotropic.

The technique used in this report can be useful in the design and evaluation of re-entry vehicle antenna systems. The rodded medium can be scaled to simulate an over dense as well as an under dense plasma sheath. An artificial dielectric can not simulate all the complexities of a re-entry plasma sheath, but at this stage the simulation of the simplest properties of a plasma can be very useful in laboratory and ground testing. A great deal of insight into the problems of re-entry communications can be gained from these simplified model studies, and it is advantageous to understand the behavior of the simplified geometries before attempting to solve the more realistic problems. Many times the simplified analysis can be used as a guide in the more complex geometries.

Dielectric Constant of a Plasma

The electromagnetic properties of a plasma can be represented by a complex dielectric constant[11,12] which has tensor properties under the application of a static magnetic field. For the purpose of this discussion, the plasma is assumed to be a homogeneous slightly ionized gas which is electrically neutral. Collisional effects are assumed to be zero and the electrons have no thermal motion. The dielectric constant for the plasma is determined by solving Maxwell's Equations in conjunction with the equation of motion of the electrons.

$$\bar{\nabla} \times \bar{E} = - j\omega \mu_o \bar{H} \tag{3}$$

$$\bar{\nabla} \times \bar{H} = j\omega \varepsilon_o \bar{E} + \bar{J} \tag{4}$$

$$\bar{J} = \rho \bar{v} \tag{5}$$

$$m \frac{d\bar{v}}{dt} = e [\bar{E} + \bar{v} \times \bar{B}] \tag{6}$$

The electron charge density is equal to ρ and the velocity of the electrons is equal to $\bar{v}$. The curl of $\bar{H}$ can also be expressed in terms of a tensor permittivity.

$$\bar{\nabla} \times \bar{H} = j\omega [\varepsilon] [\bar{E}] \tag{7}$$

If the above equations are linearized, the resulting tensor permittivity is given by

$$[\varepsilon] = \varepsilon_o[\varepsilon_r] = \varepsilon_o \begin{bmatrix} \varepsilon_{11} & j\varepsilon_{12} & 0 \\ -j\varepsilon_{12} & \varepsilon_{22} & 0 \\ 0 & 0 & \varepsilon_{33} \end{bmatrix} \tag{8}$$

when the magnetic field, B_o, is applied in the X_3 direction. The rectangular components of the tensor are equal to

$$\varepsilon_{11} = \varepsilon_{22} = 1 - \frac{\omega_p^2}{\omega^2 - \omega_c^2} \tag{9}$$

$$\varepsilon_{12} = \left(\frac{\omega_c}{\omega}\right)\left(\frac{-\omega_p^2}{\omega^2 - \omega_c^2}\right) \tag{10}$$

$$\varepsilon_{33} = 1 - \frac{\omega_p^2}{\omega^2} \tag{11}$$

$$\omega_p = \sqrt{\frac{Ne^2}{\varepsilon_o m}} = \text{plasma frequency}$$

$$\omega_c = -\frac{B_o e}{m} = \text{electron cyclotron frequency}$$

if collisional effects are neglected. It should be noted that e is a negative quantity for an electron and is equal to the electronic charge. N is the electron density, ε_o is the permittivity of free space, and m is the mass of an electron.

If the static magnetic field becomes infinite in strength, the tensor $[\varepsilon_r]$ simplifies to

$$[\varepsilon_r] = \begin{bmatrix} 1 & 0 & 0 \\ 0 & 1 & 0 \\ 0 & 0 & \left(1 - \frac{\omega_p^2}{\omega^2}\right) \end{bmatrix} ; \; B_o \to \infty \tag{12}$$

Similarly, when B_o goes to zero, the plasma becomes isotropic with a dielectric constant given by

$$\varepsilon_r = 1 - \frac{\omega_p^2}{\omega^2} \; ; \quad B_o \to 0$$

It will be shown that the above behavior is simulated by a rodded medium when there are many rods per wavelength.

II. RODDED MEDIUM

The dielectric properties of the rodded medium will be studied in this section. The rods are assumed to be perfect conducting cylinders therefore making the equivalent collision frequency zero. The electromagnetic properties of the rodded medium can be described by a macroscopic dielectric constant which has tensor characteristics. If the rods are only oriented in one direction, the rodded medium exhibits anisotropic behavior,and the propagation constant depends on the polarization of the electric field. If, however, the rods form a cubical lattice, the dielectric properties become isotropic. The spacing between adjacent rods must be much smaller than a free space wavelength. As the wavelength approaches the rod spacing, diffraction effects become dominant,and the rodded medium no longer acts like a dielectric material. Also, the air artificial dielectric interface behaves incorrectly when[13] the rod spacing becomes an appreciable portion of a wavelength.

The equivalent tensor dielectric constant for an artificial dielectric with rods in the X_3 direction only will be determined. It can be shown from symmetry arguments that the tensor permittivity of the rodded medium has the following form (see Appendix B).

$$[\varepsilon] = \varepsilon_o \begin{bmatrix} \varepsilon_{11} & 0 & 0 \\ 0 & \varepsilon_{22} & 0 \\ 0 & 0 & \varepsilon_{33} \end{bmatrix} ; \quad \varepsilon_{11} = \varepsilon_{22}$$

The rodded medium can be represented by an infinite number of periodically spaced wire gratings when propagation along the X_1 or X_2 axis is considered. This analogy leads to the equivalent

transmission line circuit[14,15,16] for the rodded medium illustrated in Figure 2. The surface impedance Z_s represents the energy storage in the vicinity of the wire gratings. If the electric field is polarized parallel to the rods, the energy near the gratings is stored in the magnetic field making the equivalent surface impedance inductive. When the electric field is perpendicular to the wires, the equivalent surface impedance is capacitive. The resulting propagation constant of the medium therefore depends on the polarization of the electric field.

The equation governing the propagation constant of a periodically loaded transmission line[17,18] with shunt impedances is given by

$$\cos Kd = \cos k_o d + j \frac{Z_o}{2Z_s} \sin k_o d , \tag{14}$$

where K is the average propagation constant of the rodded medium, k_o is the free space wave number, Z_o is the characteristic impedance of free space, and Z_s is the equivalent surface impedance of the wire gratings. First, assume the electric field is polarized in the X_3 direction. The surface impedance [19] Z_s is equal to

$$\frac{Z_{s_{||}}}{Z_o} = j \frac{d \ln \frac{d}{2\pi r}}{\lambda_o} , \tag{15}$$

where d is the distance between rods, r is the radius of the rods and λ_o is the free space wavelength. The subscript || denotes that the electric field is parallel with the wires. Equation (15) is valid when d is less than $\lambda_o/2$, and r is much less than d. When d is equal to or greater than $\lambda_o/2$, the plane of wires starts to take on the character of an optical grating and many higher order reflected beams are sometimes observed. Propagation characteristics along either the X_1 or X_2 axis are therefore determined by

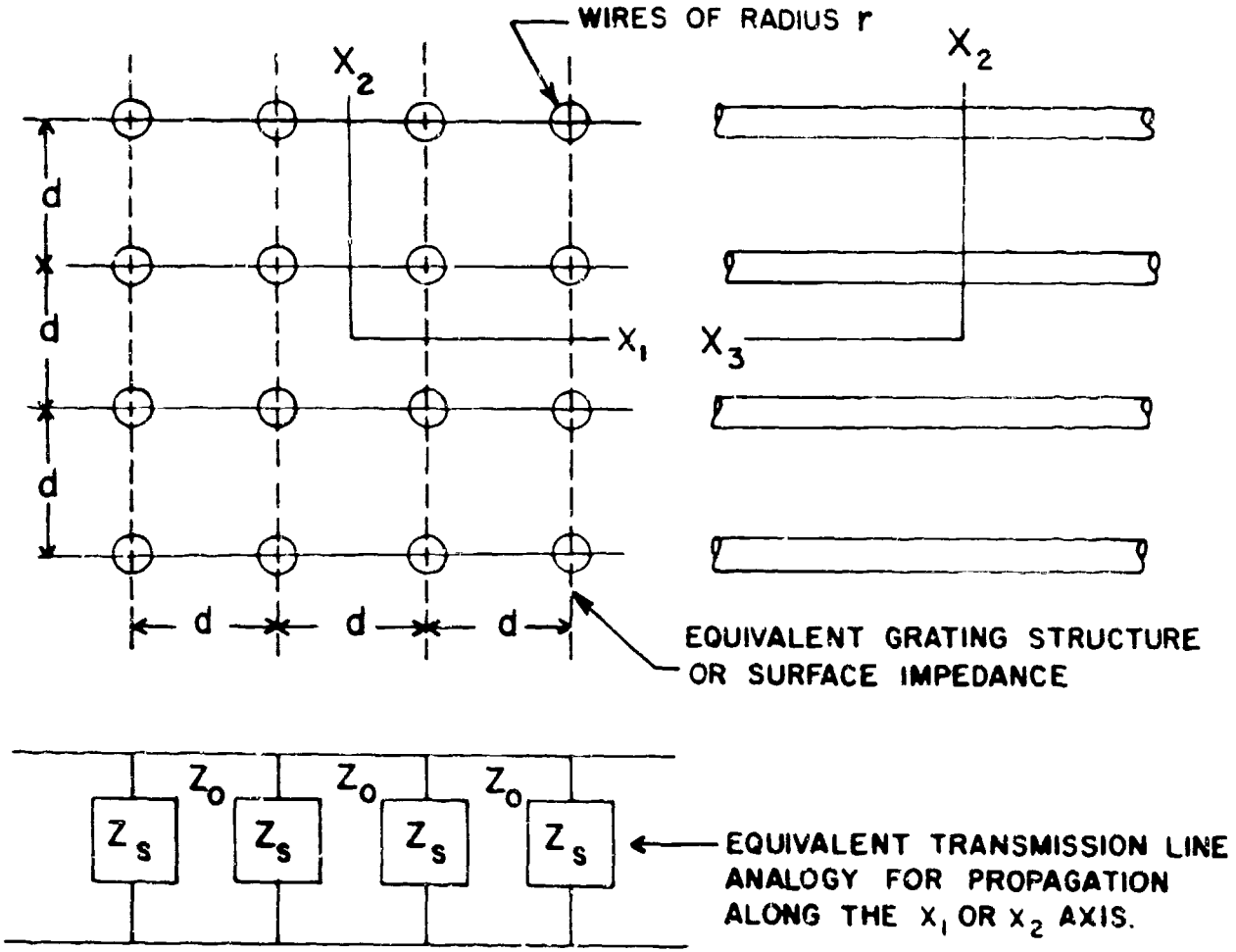

FIGURE 2 - Rodded medium geometry.

Equations (14) and (15)

$$\cos K_{\parallel} d = \cos k_o d + \frac{\lambda_o}{2d \ln\left(\frac{d}{2\pi r}\right)} \sin k_o d \tag{16}$$

so long as the electric field is parallel to the X_3 axis. Equation (16) can be simplified if $k_o d$ is assumed to be much less than unity. Then the above expression deduces to

$$\frac{K_{\parallel}^2}{k_o^2} = 1 - \frac{\lambda_o^2}{2\pi d^2 \ln\left(\frac{d}{2\pi r}\right)} . \tag{17}$$

The relationships between the propagation constant $K_{\parallel}$ and the tensor dielectric constant $[\varepsilon]$ are shown in Table (1a) in Appendix A. For the above conditions, the propagation constant, $K_{\parallel}^2$, is equal to

$$\frac{K_{\parallel}^2}{k_o^2} = \varepsilon_{33} . \tag{18}$$

The combination of Equations (17) and (18) yields

$$\varepsilon_{33} = 1 - \frac{\lambda_o^2}{2\pi d^2 \ln\left(\frac{d}{2\pi r}\right)} . \tag{19}$$

If, however, $k_o d$ is greater than 0.1, ε_{33} should be determined from Equations (16) and (18).

Now, assume that the electric field is parallel to X_1 axis and propagation is in the X_2 direction. For this polarization the equivalent surface impedance[20] Z_s is given by

$$\frac{Z_{s\perp}}{Z_o} = \frac{\lambda_o d}{j(2\pi r)^2} \tag{20}$$

The subscript $\perp$ denotes that the electric field is perpendicular to the wires. Equation (20) is valid when the ratio r/d is much less than unity. The equation governing the propagation constant for this polarization is obtained by substituting Equation (20) into Equation (14).

$$\cos K_\perp d = \cos k_o d - \frac{(2\pi r)^2}{2\lambda_o d} \sin k_o d \tag{21}$$

Equation (21) reduces to

$$\frac{K_\perp^2}{k_o^2} = 1 + \frac{2\pi r^2}{d^2} \tag{22}$$

when $k_o d$ is much less than unity. The value of $K_\perp^2$ is again obtained from Table (1a) in Appendix A

$$\frac{K_\perp^2}{k_o^2} = \epsilon_{11} \tag{23}$$

and is combined with Equation (22) to yield

$$\epsilon_{11} = 1 + \frac{2\pi r^2}{d^2} \tag{24}$$

It is interesting to note that Equation (24) can be deduced by using the concept of electric polarizability of the rods[21]. This approach is equivalent to the techniques used in determining the

dielectric constant of a molecular medium[22,23].

For most practical cases, the ratio r/d is extremely small, typically, ranging from 10^{-2} to 10^{-3}. Under these conditions, Equation (24) reduces to

$$\varepsilon_{11} \approx 1 \; ; \quad r^2/d^2 \ll 1 \; . \tag{25}$$

In a similar manner, ε_{22} is also equal to unity. The resulting dielectric tensor for an artificial dielectric with rods in the X_3 direction is

$$[\varepsilon] = \begin{bmatrix} 1 & 0 & 0 \\ 0 & 1 & 0 \\ 0 & 0 & \left(1 - \lambda_o^2/\lambda_p^2\right) \end{bmatrix} \varepsilon_o \tag{26}$$

where

$$\lambda_p^2 = 2\pi d^2 \ \ln \left(\frac{d}{2\pi r}\right) \; . \tag{27}$$

When the ratio d/λ_o is between 0.02 and 0.5, Equations (16) and (18) can be used to determine ε_{33}.

Equation (26) resembles the tensor dielectric constant of an anisotropic plasma with an infinite static magnetic field applied in the X_3 direction.

$$[\epsilon] = \begin{bmatrix} 1 & 0 & 0 \\ 0 & 1 & 0 \\ 0 & 0 & \left(1 - \omega_p^2/\omega^2\right) \end{bmatrix} \epsilon_o \tag{28}$$

The λ_p of the rodded medium is therefore the analogue of the cutoff wavelength in the plasma.

When the plasma is subjected to an infinite magnetostatic field, the oscillating electron currents in the plasma are confined to flow along the magnetic lines of force. In a similar manner, the oscillatory currents in the rodded medium are confined to flow along the wires thereby simulating the effect of applying an infinite steady magnetic field to the plasma.

The tensor dielectric constant for an artificial dielectric having rods parallel to both the X_2 and X_3 axis is given by

$$[\epsilon] = \begin{bmatrix} 1 & 0 & 0 \\ 0 & \left(1 - \lambda_o^2/\lambda_p^2\right) & 0 \\ 0 & 0 & \left(1 - \lambda_o^2/\lambda_p{}^2\right) \end{bmatrix} \epsilon_o \, . \tag{29}$$

Similarly, the tensor dielectric constant for a cubical array of rods is equal to

$$[\epsilon] = \begin{bmatrix} \left(1 - \lambda_o^2/\lambda_p^2\right) & 0 & 0 \\ 0 & \left(1 - \lambda_o^2/\lambda_p^2\right) & 0 \\ 0 & 0 & \left(1 - \lambda_o^2/\lambda_p^2\right) \end{bmatrix} \epsilon_o \, . \tag{30}$$

Since all the diagonal terms are equal, the medium is isotropic and the dielectric constant is given by

$$\varepsilon = \left(1 - \lambda_o^2/\lambda_p^2\right) \varepsilon_o \quad . \tag{31}$$

The equivalent index of refraction, n, for an isotropic rodded medium is obtained from an alternate form of Equation (16).

$$\cos\left(\frac{2\pi nd}{\lambda_o}\right) = \cos\left(\frac{2\pi d}{\lambda_o}\right) + \frac{\lambda_o}{2d \ln\left(\frac{d}{2\pi r}\right)} \sin\left(\frac{2\pi d}{\lambda_o}\right) \tag{32}$$

The index of refraction of the medium is defined by

$$n = \lambda_o/\lambda \quad , \tag{33}$$

where λ is the average wavelength in the rodded medium. The index of refraction, as given in Equation (32), can be approximated by

$$n = \left(1 - \lambda_o^2/\lambda_p^2\right)^{1/2} \quad , \tag{34}$$

where λ_p is the largest zero of $F(\lambda)$

$$F(\lambda) \equiv 1 - \left[\cos\left(\frac{2\pi d}{\lambda_o}\right) + \frac{\lambda_o}{2d \ln\left(\frac{d}{2\pi r}\right)} \sin\left(\frac{2\pi d}{\lambda_o}\right)\right] = 0. \tag{35}$$

Equation (35) is the result of setting n equal to zero in Equation (32). λ_p is therefore the longest cutoff wavelength of the rodded medium. When the spacing constant d is much smaller than a wavelength, the equivalent plasma wavelength reduces to the value given in Equation (27).

$$\lambda_p^2 = 2\pi d^2 \ln\left(\frac{d}{2\pi r}\right) \tag{36}$$

The theoretical values of n for the rodded medium used in the experimental study are shown in Figure 3. The pertinent quantities pertaining to the experimental geometry are given below

$$d = 0.3 \text{ in.}$$
$$r = 0.002 \text{ in.}$$
$$\text{freq range} = 8 \text{ to } 12 \text{ kmc.}$$

In general, the rodded medium behaves like a homogeneous isotropic plasma when the rods form a cubical lattice structure. In certain idealized geometries, however, the cubical lattice structure is not necessary. For example, the reflection and transmission characteristics of a plasma slab at normal incidence can be simulated by orienting the rods in the direction of the incident electric field. Physically, rods tend to simulate the effects of the oscillatory motions of the free electrons in the plasma. If any of the rectangular components of the electric field are zero throughout the plasma region, the rods oriented in those directions can be eliminated since they are not involved in the simulation.

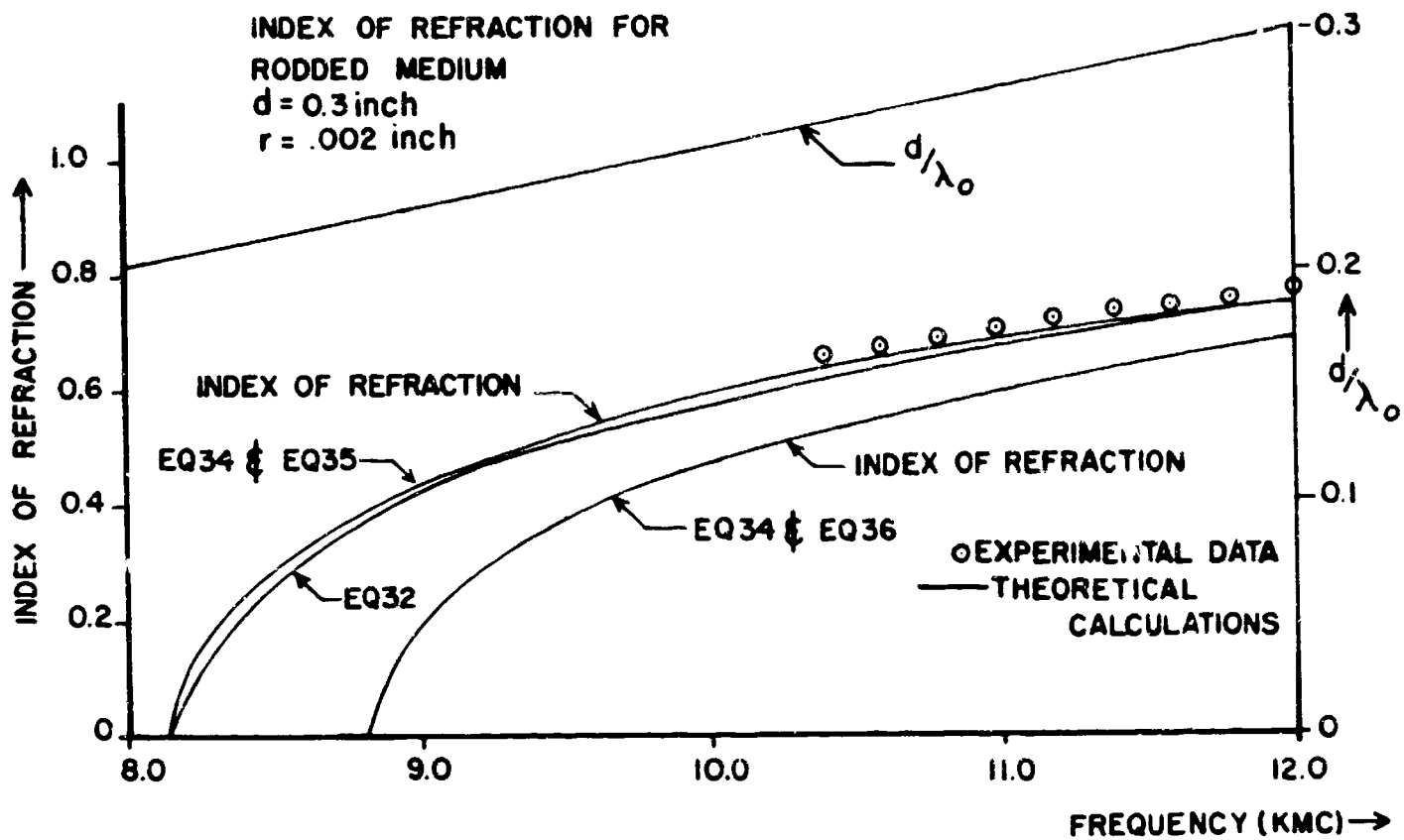

FIGURE 3 - Characteristics of the rodded medium.

III. EXPERIMENTAL STUDY

Waveguide Measurements

The propagation characteristics of a rodded medium similar to the ones used in the pattern measurements have been measured in an X-band waveguide interferometer shown in Figure 4. The dominant TE_{10} mode in a rectangular waveguide is analogous to two uniform plane waves bouncing off the walls of the waveguide, as shown in Figure 5. The equivalent angle of incidence, θ, of these waves is related to the wav guide wavelength and is given by[24]

$$\lambda_o/\lambda_g = \cos\theta , \tag{37}$$

where λ_g is the waveguide wavelength. The equivalent angle of incidence can also be given in terms of the cutoff wavelength[25] of the X-band waveguide,

$$\lambda_o/\lambda_c = \sin\theta . \tag{38}$$

The waveguide measurements are equivalent to the same measurements performed in free space at an angle of incidence given by Equation (38).

The relative dielectric constant of the rodded medium can be related to the absolute fringe shifts measured with the interferometer. The relative fringe shift, $\Delta\alpha_{rel}$, is given by

$$\Delta\alpha_{rel} = \theta_{NL} - \theta_L , \tag{39}$$

where θ_{NL} is the reading on the calibrated phase shifter in the absence of the sample and θ_L is the reading on the phase shifter in the presence of the sample. The absolute value of the fringe

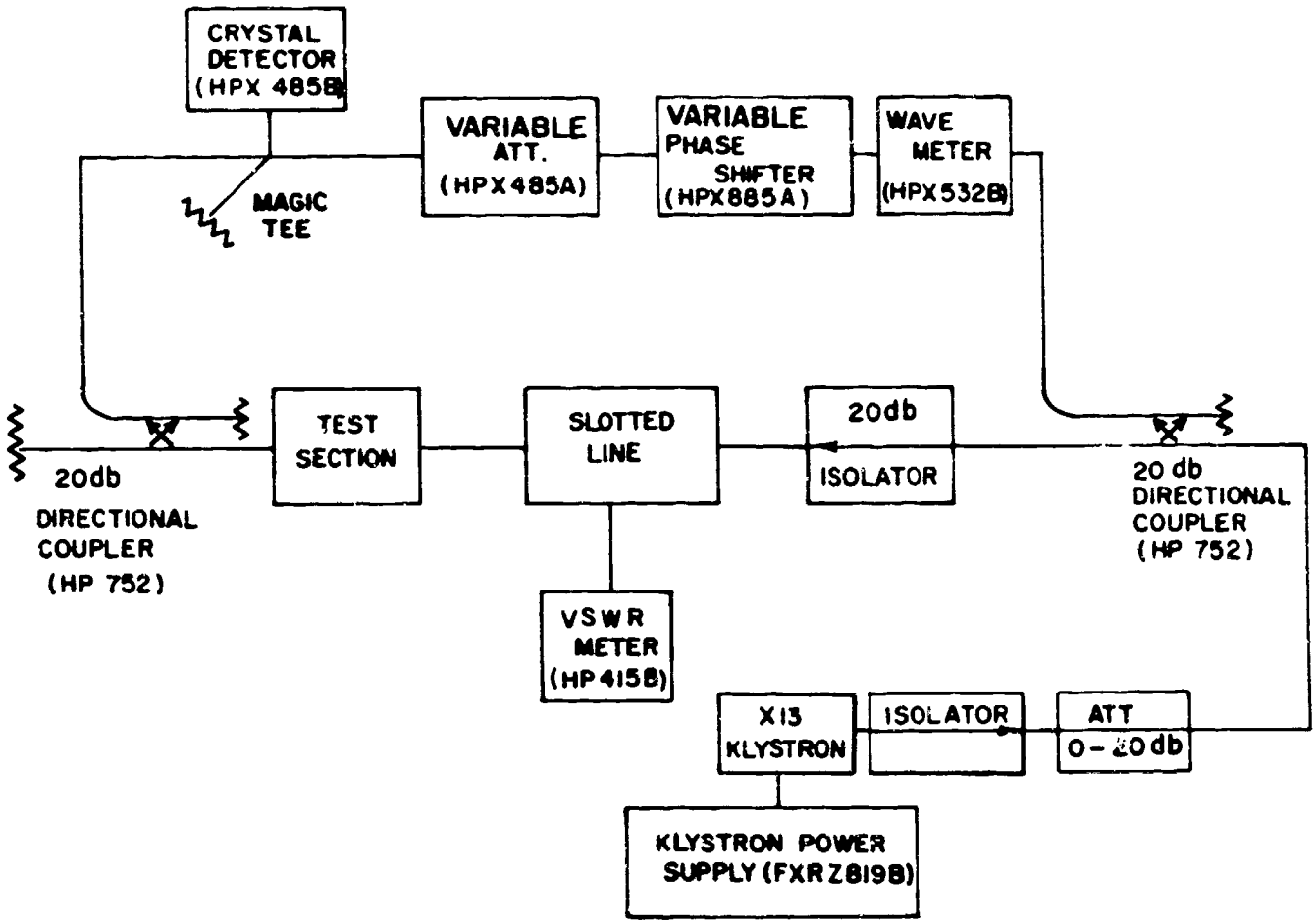

FIGURE 4 - Diagram of the X-band waveguide interferometer.

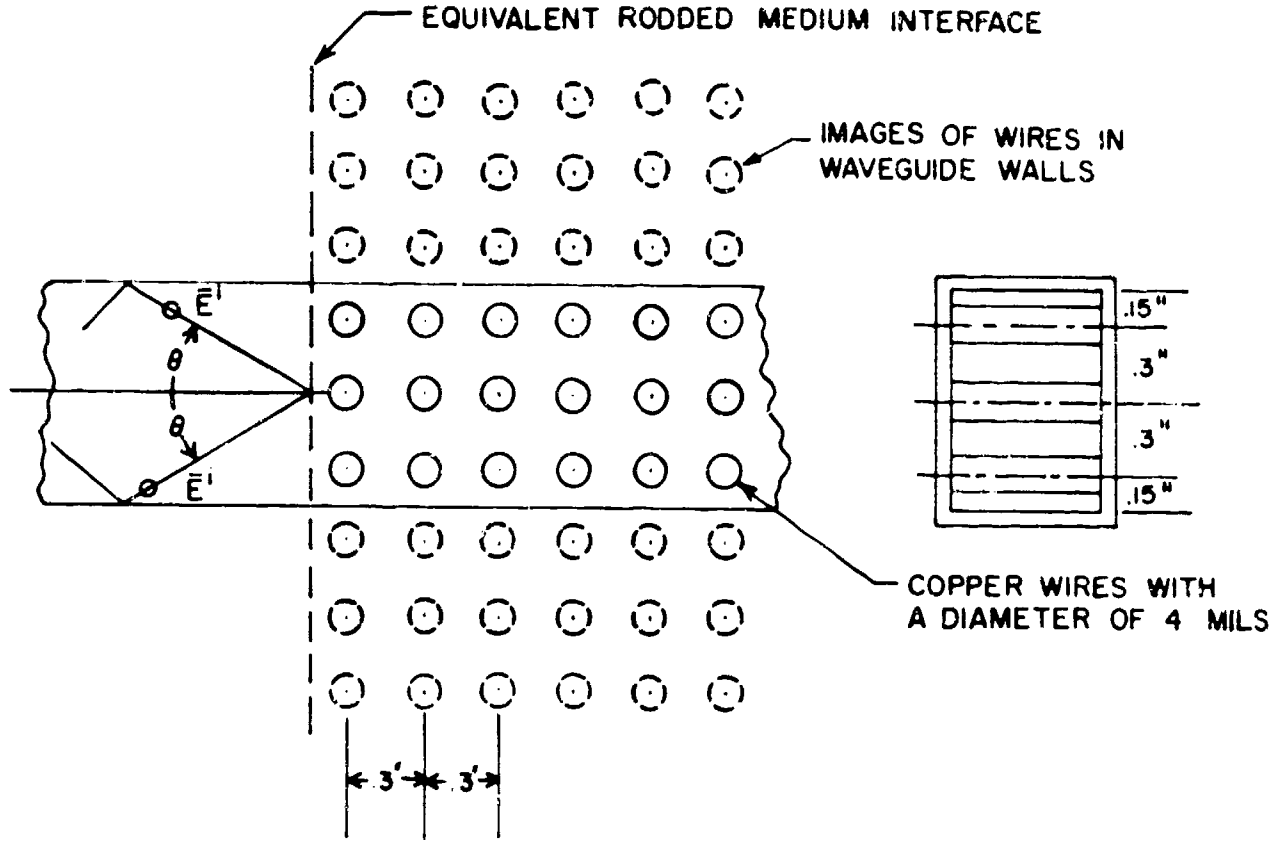

FIGURE 5 - Rodded medium in waveguide geometry.

shift is given by

$$\Delta\alpha = \Delta\alpha_{rel} \pm M2\pi , \tag{40}$$

where M is an integer. The ambiguity in the measured value of $\Delta\alpha$ stems from the inability of the relative phase shift measurements to distinguish multiples of 2π. The value of M can be determined by estimating the relative dielectric constant, ε_r, or by performing an additional set of measurements with a different length sample.

The measured value of $\Delta\alpha$ can also be related to

$$\Delta\alpha = (\beta_{10} - \beta_z)\ell , \tag{41}$$

where β_{10} is the propagation constant of the empty waveguide, β_z is the propagation constant of the loaded waveguide, and ℓ is the length of the sample. Equation (41) is only approximate in that the phase shifts attributed to the multiple reflections off the ends of the sample are neglected. When the magnitude of the reflection coefficient is small, the measured transmission phase given by Equation (40) approaches the value given by Equation (41).

The propagation constant of the loaded waveguide is equal to[26]

$$\beta_z = \sqrt{k_o^2 \varepsilon_r - \left(\frac{2\pi}{\lambda_c}\right)^2} \quad ; \ TE_{10} \text{ mode} \tag{42}$$

where ε_r is the relative dielectric constant of the sample, and λ_c is the cutoff wavelength of the unloaded waveguide. Equation (42) can be rewritten in the form

$$\varepsilon_r = \left(\frac{\beta_z}{k_o}\right)^2 + \left(\frac{\lambda_o}{\lambda_c}\right)^2 . \tag{43}$$

It is interesting to note that Equation (43) can be obtained from Snell's Law when the angle of incidence is given by Equation (38),

$$\varepsilon_r = \left(\frac{\beta_z}{k_o}\right)^2 + \sin^2\theta \tag{44}$$

which again illustrates the analogy between the waveguide and the free space measurements.

The results of the measurements performed on the rodded medium used in the antenna pattern measurements are shown in Figure 3. The measured index of refraction corresponds to the case with the electric field parallel to the wires.

Additional measurements were performed with the wires oriented perpendicular to the electric field. In one case the wires were oriented in the transverse plane but perpendicular to the electric field, and in the other the wires were oriented in the direction of propagation. These measurements indicated no apparent phase shift due to the presence of the wires, making the equivalent index of refraction for these polarizations equal to unity. The behavior of a rodded medium with the wires oriented in one direction, therefore, exhibited the anisotropic properties described in the previous section when viewed in the X-band waveguide geometry.

The surface impedance of a single plane of wires was measured with the aid of the slotted line shown in Figure 4. The wires were oriented in the direction of the electric field, and the experimental data and theoretical model were within 10%, as shown in Figure 6. Better agreement was obtained by using a one point fit between theory and experiment. In other words, the equivalent surface inductance of the plane of wires was obtained experimentally.

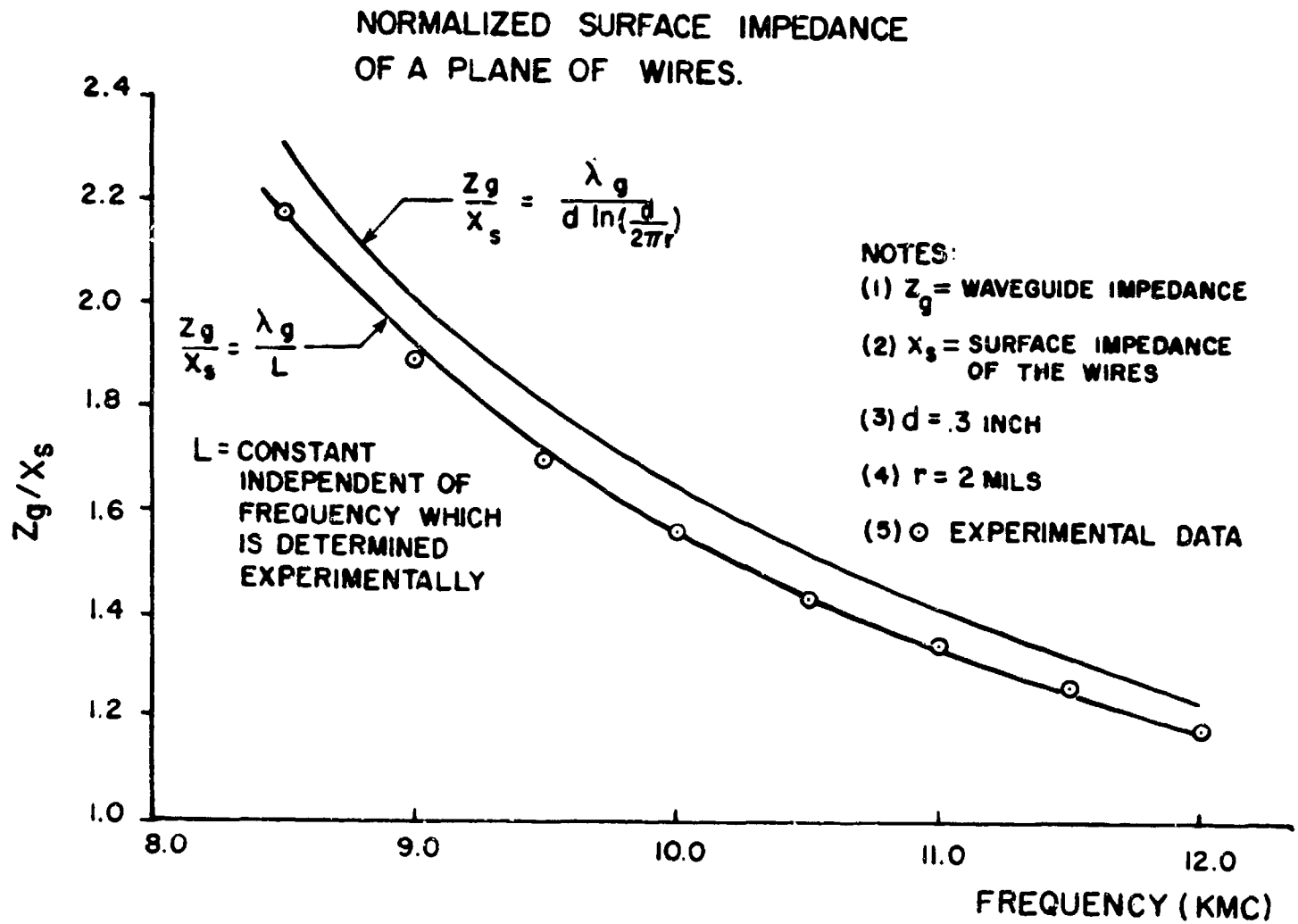

FIGURE 6 - Surface impedance of a single plane of equally spaced wires.

Antenna Geometry

The radiation patterns from an X-band horn, terminated in an infinite ground plane, which was radiating through an unbounded homogeneous plasma sheath, were measured experimentally (see Figure 1). The sheath was assumed to be under-dense or operating above the plasma frequency. The actual experimental antenna geometry only approximated the idealized model described above. The sheath was simulated by an artificial dielectric slab which was large compared with the dimensions of the antenna aperture and slab thickness. The restrictions on the size of the slab were a necessary requirement for the slab to approximate an unbounded layer. For this particular experimental study, the aperture size was given by

$$a = 3.25 \text{ inches}$$
$$b = 2.625 \text{ inches},$$

and the dimensions of the ground plane were about six times greater than the dimensions of the aperture. The axial length of the horn was 12 inches.

The horn was excited with a TE_{10} mode which is equivalent to having the following aperture distribution

$$\bar{E}\ (z = 0) = \bar{u}_y\ E_o \cos \frac{\pi x}{a}$$

developed in the mouth of the horn.

Design of the Rodded Medium

Two artificial dielectric geometries were utilized in the pattern measurements. Both models were constructed with 38 gauge wire and a wire spacing of 0.3 inch. The equivalent plasma frequency of the artificial dielectrics was 8.1 KMC..

The majority of the measurements were performed with the rodded medium shown in Figures 7, 8 and 9. The equivalent thickness of the slab could be varied from 0 to 3 inches in 0.3 inch steps. In this geometry the wires were oriented in the Y direction and were held in position by the grooved posts located at the top and bottom of the ground plane. Wire sag was eliminated by keeping the wires under tension. The springs located near the upper edge of the ground plane maintained the desired tension in the wires. Microwave absorbing material was placed around the posts and associated hardware to eliminate scattering problems. The absorbing material altered the measured E plane patterns at angles greater than 50 degrees, but these effects were far less severe than the ones occurring when the absorbing material was absent. The H plane patterns were practically unaltered by the presence of the absorber.

Figure 10 shows the effects produced by the absorbing material. The dashed curve in Figure 10 represents the E plane pattern of the apparatus shown in Figure 9, and the solid curve is the E plane pattern of the horn and ground plane alone.

The validity of this rodded medium model is a function of the specific antenna geometry being simulated. If the Y components of the induced currents are producing the dominant pattern changes, the rodded medium described above is adequate for the simulation. In principle, when the horn aperture is large compared with a wavelength and the thickness of the sheath is small compared to the aperture, the majority of the oscillatory currents in the plasma can be assumed to be directed along the Y axis. These arguments are valid when the angle θ is not too large. The Z components of the currents become increasingly important as θ approaches 90 degrees in the E plane.

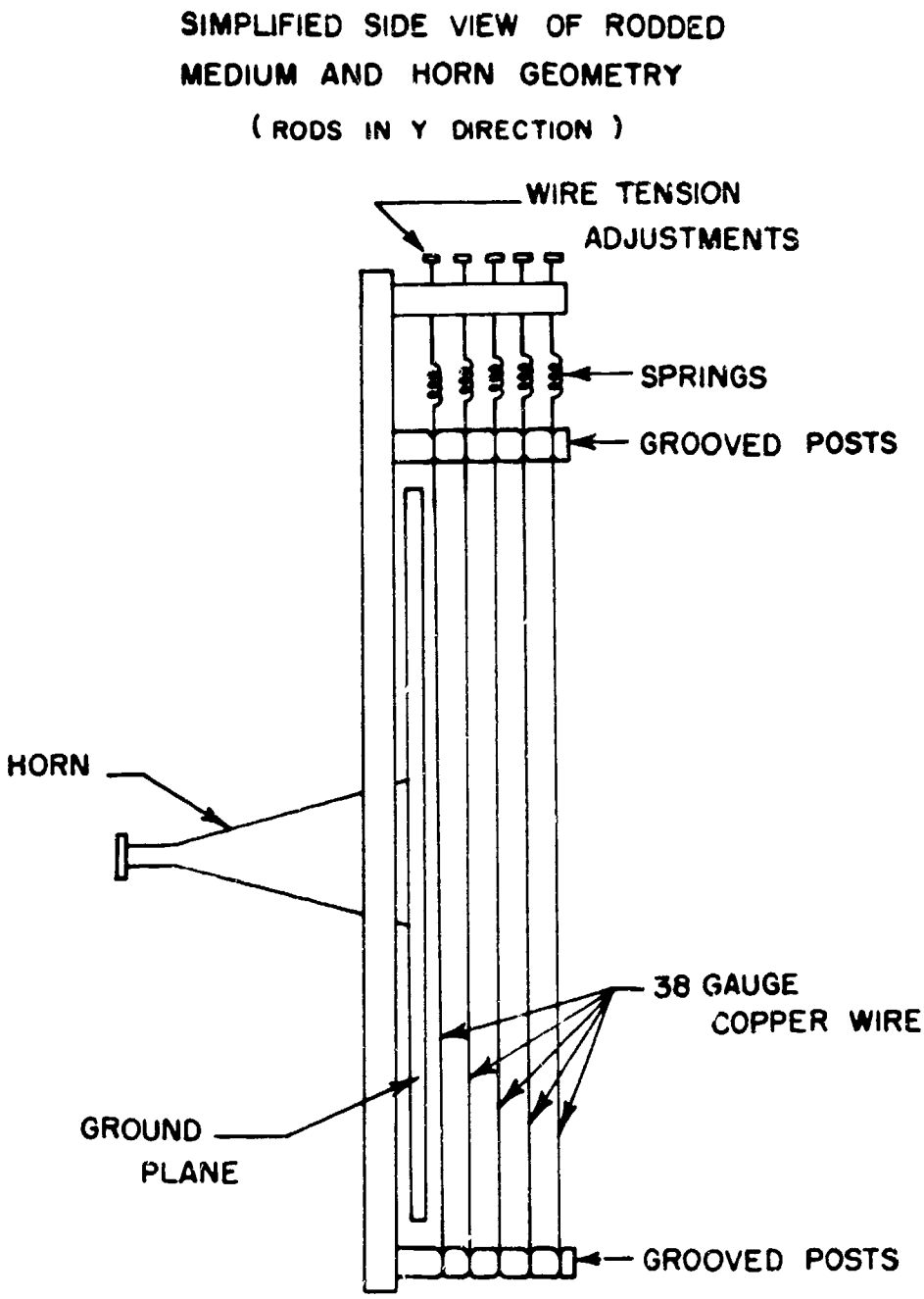

FIGURE 7 - Antenna geometry with rods oriented in the Y direction.

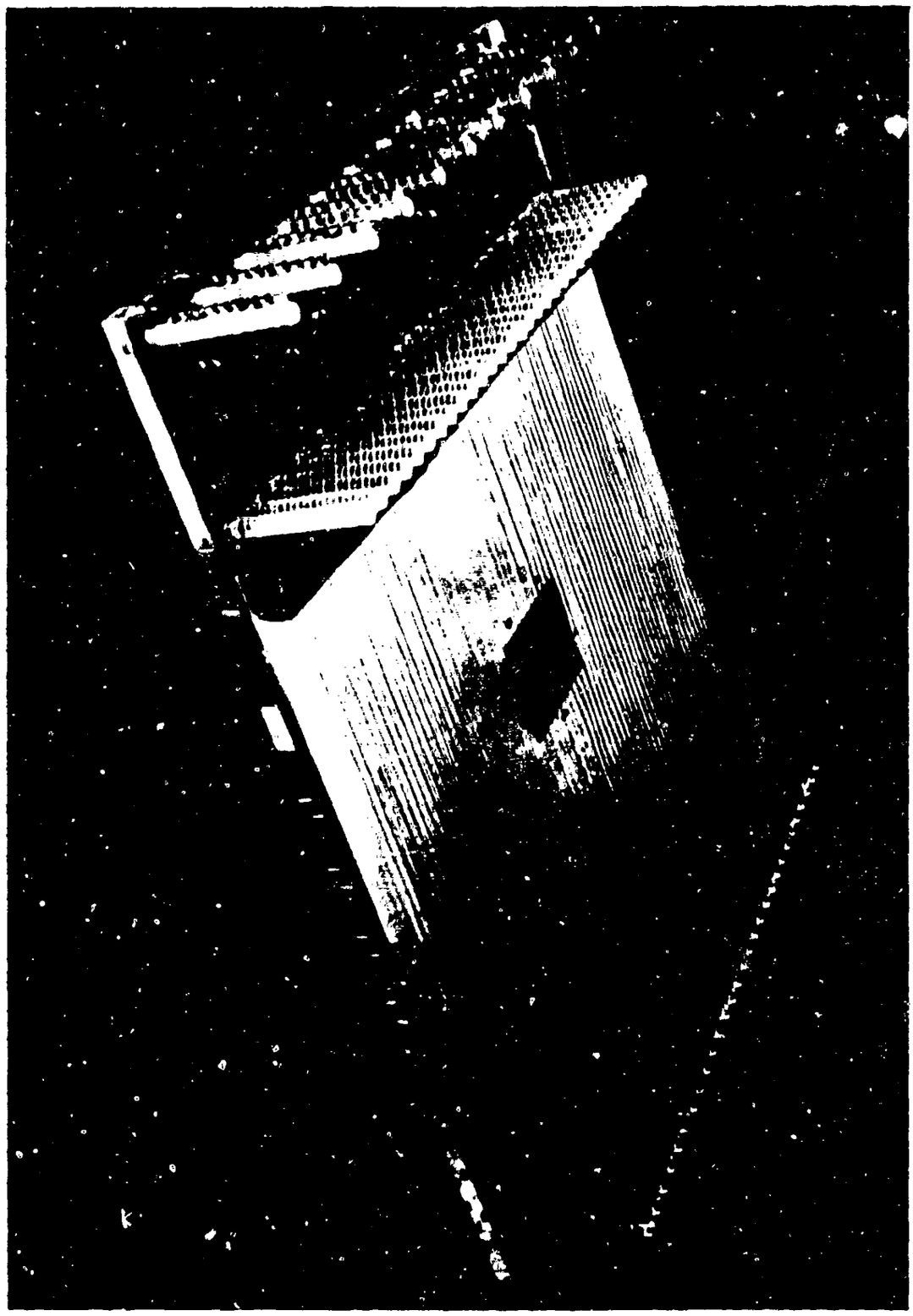

Figure 8. Experimental antenna geometry without the absorbing material (rods in the Y direction).

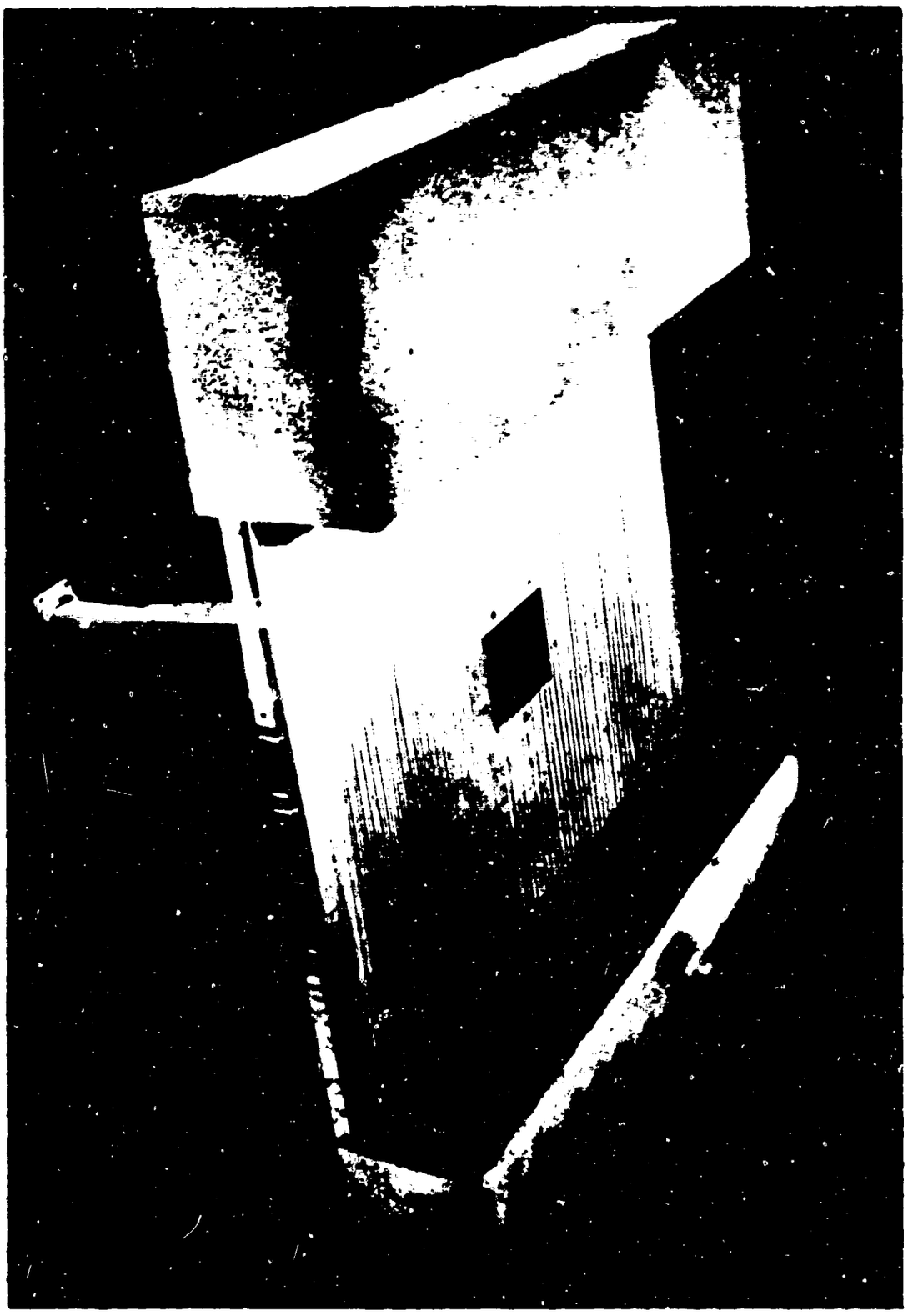

Figure 9. Experimental antenna configuration with the absorbing material (rods in the Y direction).

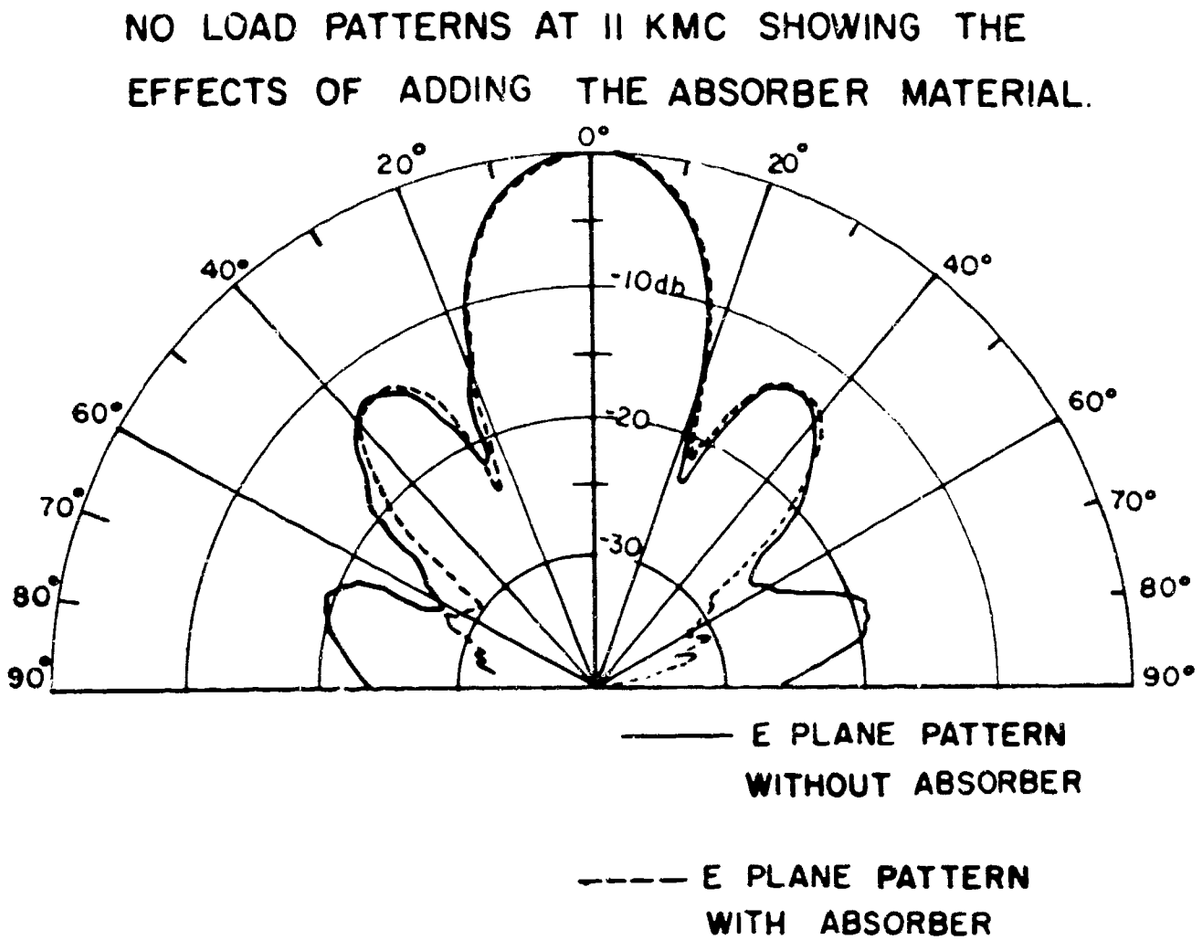

FIGURE 10 - Radiation patterns with and without the absorbing material.

Since there are currents flowing in the Z direction in this antenna geometry, an improvement in the simulation of a homogeneous isotropic plasma layer was accomplished by orienting the wires in both the Y and Z directions. The wires parallel to the X axis were omitted on the premise that the currents excited in the X direction produce little or no effects in the E and H plane measurements. The wire mesh structures used in the fabrication of this artificial dielectric were held in position by styrofoam spacers (see Figure 11). Similar techniques have been utilized in the construction of artificial dielectric lenses[27]. The thickness of this slab was 2.7 inches, and the equivalent plasma frequency was 8.1 KMC. The experimental antenna is shown in Figure 12.

Pattern Measurements

The radiation patterns were measured on a laboratory apparatus shown in Figure 13. The probe antenna, which was supported by a movable plywood arm, was operated as a receiving antenna. The transmission path between the transmitting and receiving antennas was 6 feet and the angular position of the movable arm with respect to the axis of the transmitting horn could be varied from 0 degrees to 90 degrees in 5 degree increments. It became apparent that the angular resolution of this apparatus was inadequate for this particular experiment and some of the fine structure of the patterns was not detected.

In order to obtain better angular resolution, the measurements were performed on a free space antenna range shown in Figure 14. The antenna positioner was equipped to rotate in both the θ and ϕ directions. The transmitting source or probe horn was mounted on a stationary non-reflecting pole located about 30 feet from the receiving antenna at a height of 17 feet. The free space range was instrumented to measure the receiving patterns of an antenna system.

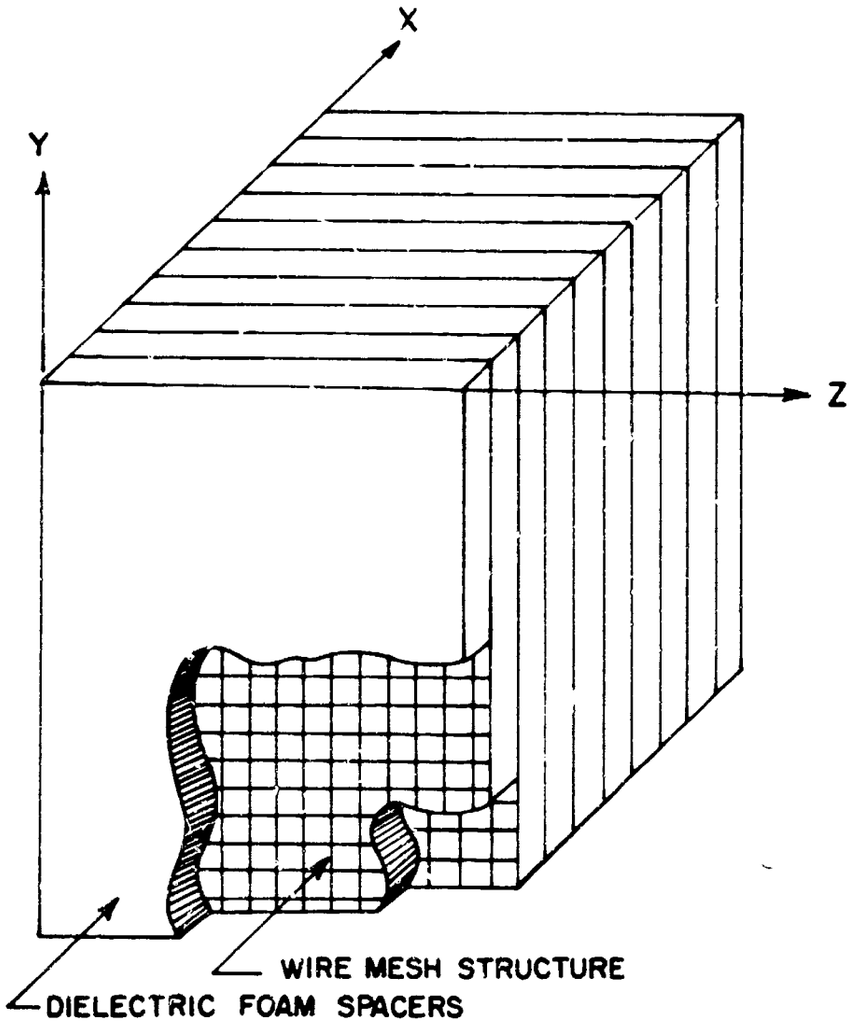

THE ARTIFICAL DIELECTRIC SHOWN IN THIS DIAGRAM IS CONSTRUCTED WITH THE WIRE MESH STRUCTURE SANDWICHED BETWEEN DIELECTRIC FOAM SPACERS. THE FOAM SPACERS ARE GLUED TOGETHER, THEREBY HOLDING THE WIRES IN PLACE. IT SHOULD BE NOTED THAT THE WIRES NEED NOT MAKE ELECTRICAL CONTACT AT JUNCTION POINTS.

FIGURE 11 - Rodded medium with rods in both the Y and Z directions.

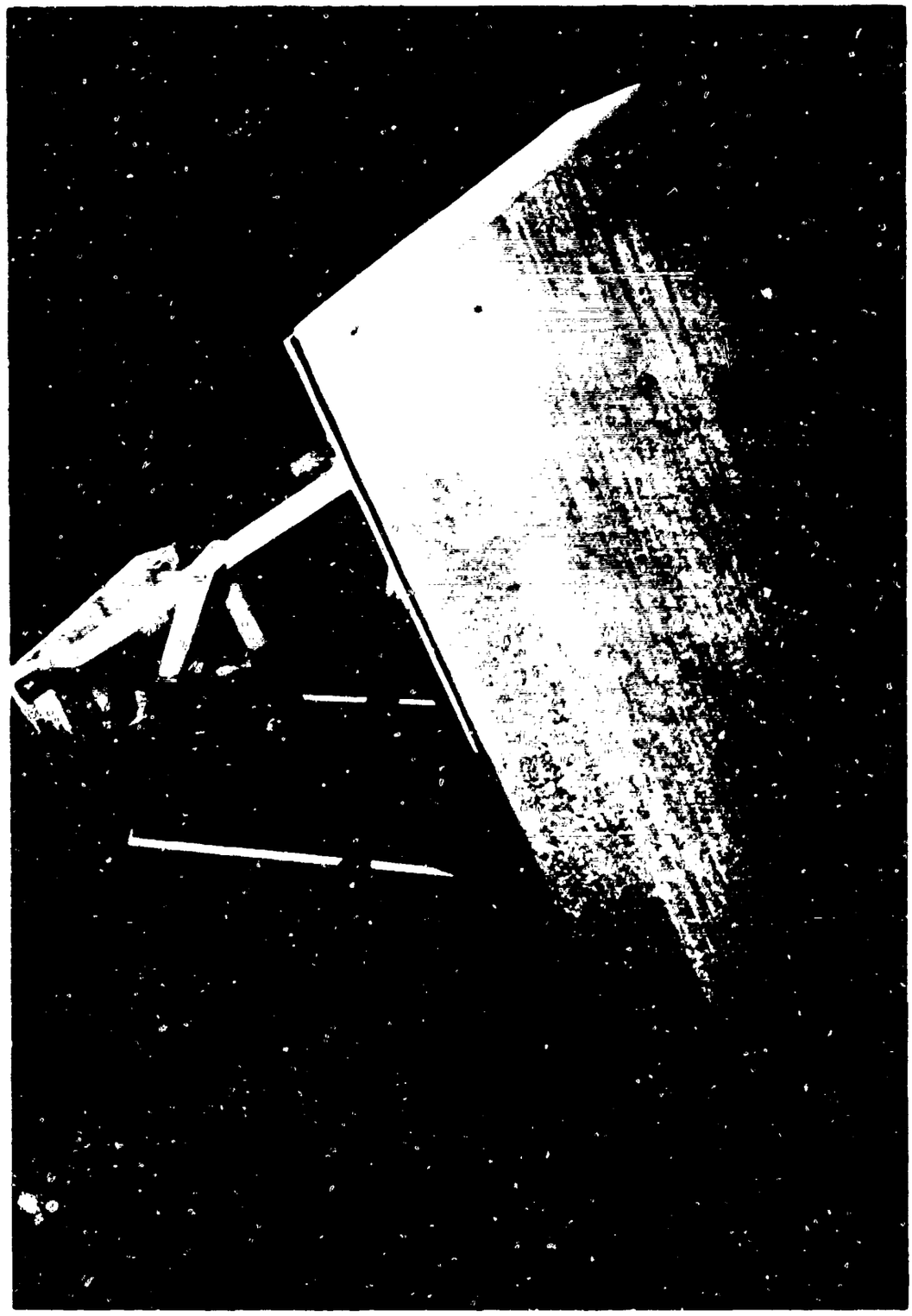

Figure 12. Experimental antenna geometry using the rodded medium shown in Figure 11 (rods in both the Y and Z direction).

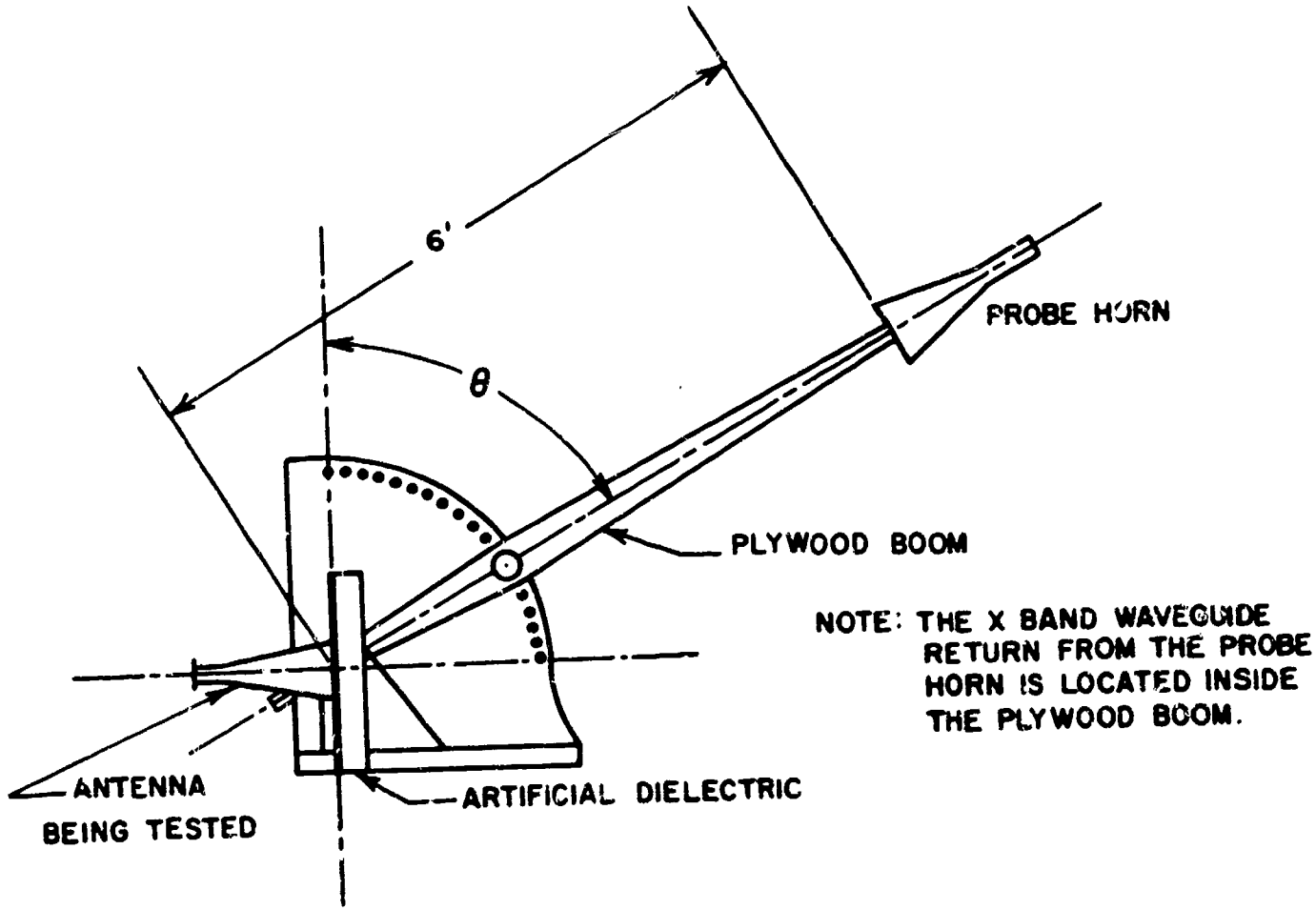

FIGURE 13 - Laboratory pattern range.

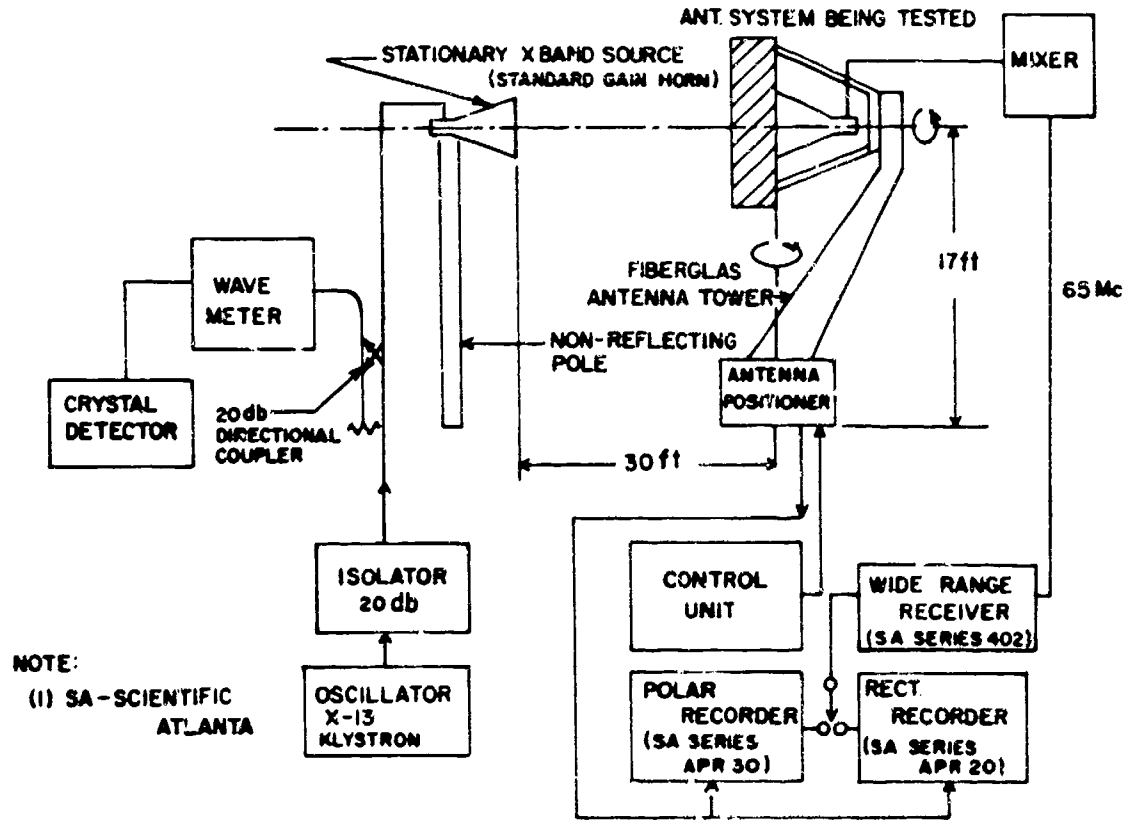

FIGURE 14 - Block diagram of the free space antenna range.

However, if the probe horn and antenna being tested are loosely coupled and the driving point impedances are independent of angular position, by reciprocity the receiving and transmitting patterns are equal.[28] Figure 15 illustrates the comparison between the patterns measured with the laboratory apparatus and a free space antenna range.

The E and H plane patterns of the horn antenna with and without the artificial dielectric were measured at 9, 10 and 11 KMC. Both rodded media were used in the measurements. The patterns obtained with the apparatus shown in Figure 9 are displayed in Figures 16 through 22. The two slab thicknesses chosen for these tests were 1.5 inches and 2.1 inches. The experimental measurements were compared with the theoretical calculations of the appropriate slit problem referred to in the introduction. The E plane patterns were compared with Equation (1) and the H plane patterns were compared with Equation (2).

Equations (1) and (2) can be factored into two functions, one being associated with the pattern without the plasma sheath and the other being associated entirely with the plasma sheath. The resulting patterns can be expressed as

$$\text{E Plane;} \quad P_\theta = L_\phi^2 \; A_\theta A_\theta^* \tag{45}$$

$$\text{H Plane;} \quad P_\phi = L_\theta^2 \; A_\phi A_\phi^* \tag{46}$$

where

$$L_\phi = \frac{\sin\left(\frac{k_o b}{2} \sin\theta\right)}{\frac{k_o b}{2} \sin\theta} \tag{47}$$

$$L_\theta = \frac{\pi^2}{4} \left[\frac{\cos\left(\frac{k_o a}{2} \sin\theta\right) \cos\theta}{\left(\frac{\pi}{2}\right)^2 - \left(\frac{k_o a}{2} \sin\theta\right)^2} \right] \tag{48}$$

$$A_\theta A_\theta^* = \frac{1}{\cos^2(K_z \ell) + \frac{1}{n^4}\left(\frac{n^2 - \sin^2\theta}{\cos^2\theta}\right)\sin^2(K_z \ell)} \tag{49}$$

$$A_\phi A_\phi^* = \frac{1}{\cos^2(K_z \ell) + \left(\frac{\cos^2\theta}{n^2 - \sin^2\theta}\right)\sin^2(K_z \ell)} \tag{50}$$

$$K_z = k_o \sqrt{n^2 - \sin^2\theta} \tag{51}$$

$$n = \left(1 - \frac{\omega_p^2}{\omega}\right)^{1/2} \tag{52}$$

ℓ = thickness of the sheath. (53)

The functions L_ϕ and L_θ are respectively the E plane and H plane patterns of a horn in an infinite ground plane. Figures 23 and 24 summarize the experimentally determined values of $A_\phi A_\phi^*$ and the corresponding theoretical computation obtained from Equation (50). The experimental values of $A_\phi A_\phi^*$ are obtained by dividing the composite H plane pattern of the horn and artificial dielectric by the H plane pattern of the horn alone.

The E plane patterns obtained with the apparatus shown in Figure 12 are given in Figures 25 and 26. The artificial dielectric used in these measurements had rods oriented in both the Y and Z directions, and the equivalent thickness of the simulated plasma sheath was 2.7 inches. Again the experimental measurements were compared with Equation (1).

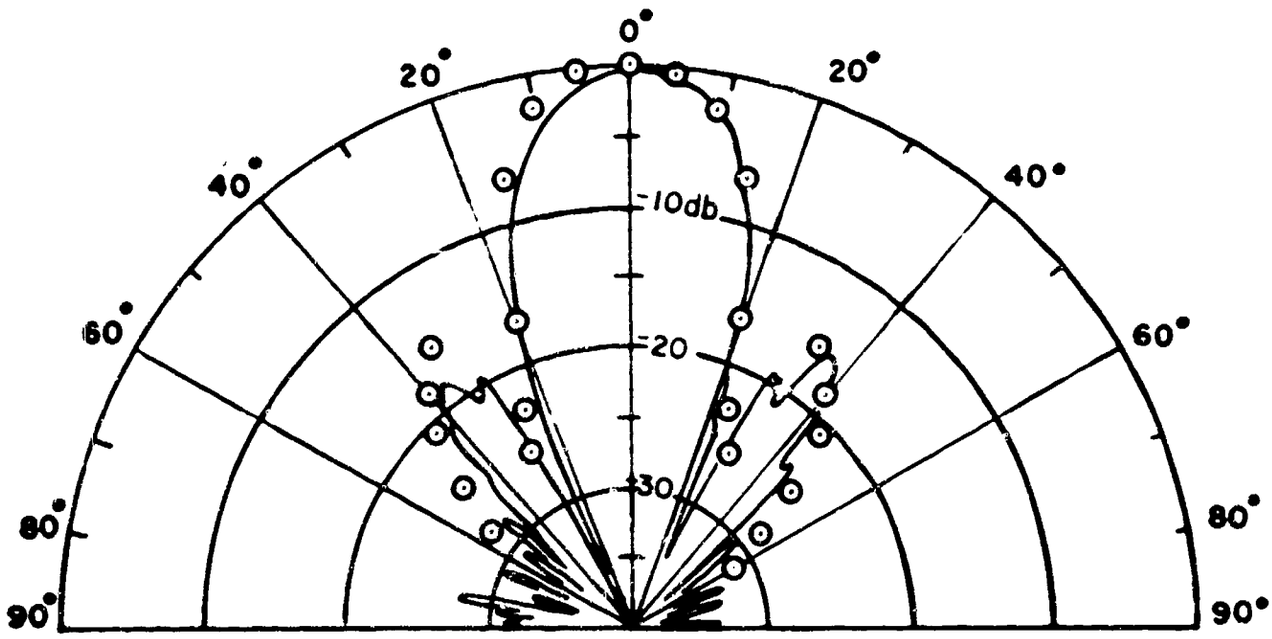

NOTES: (1) f = 11.3 KMC

(2) f_p = 8.1 KMC

(3) ℓ = 1.5 inches

—— FREE SPACE RANGE

⊙⊙⊙ LABORATORY RANGE

FIGURE 15 - Comparison between the radiation patterns measured with the laboratory and free space pattern ranges.

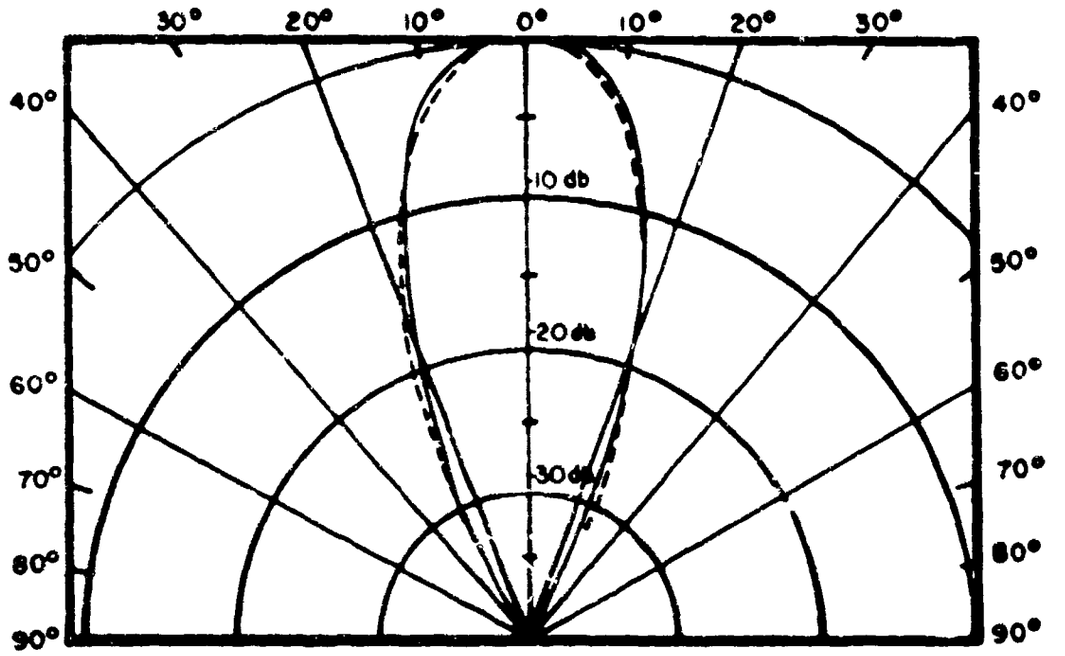

ℓ = 1.5 in, f = 9 KMC, f_p = 8.1 KMC

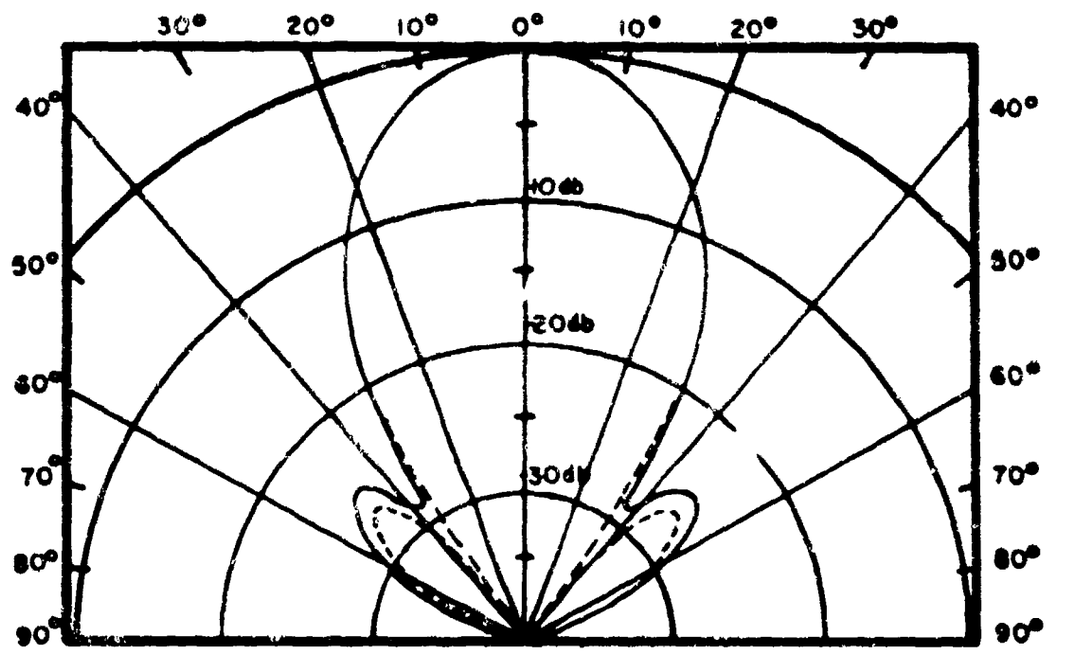

ℓ = 0, no plasma, f = 9 KMC

— EXPTL. DATA

----THEORY (REF. 2, n = .426)

FIGURE 16 - H plane radiation patterns of the antenna shown in Fig. 9 at 9 KMC (rods in the Y direction).

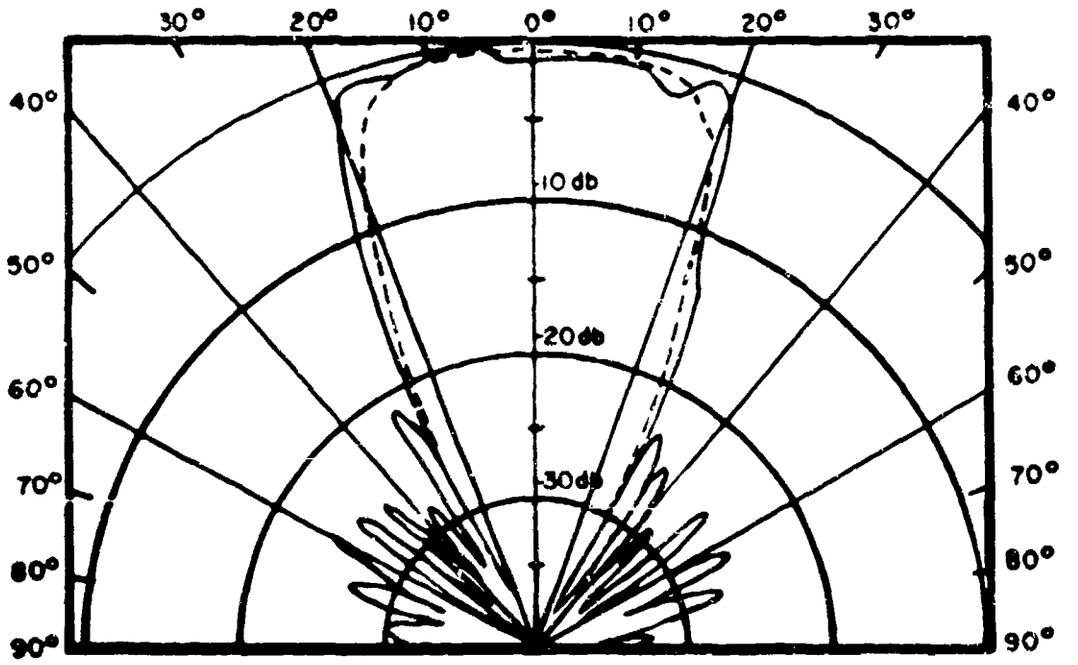

ℓ = 2.1", f = 9 KMC, f_p = 8.1 KMC,

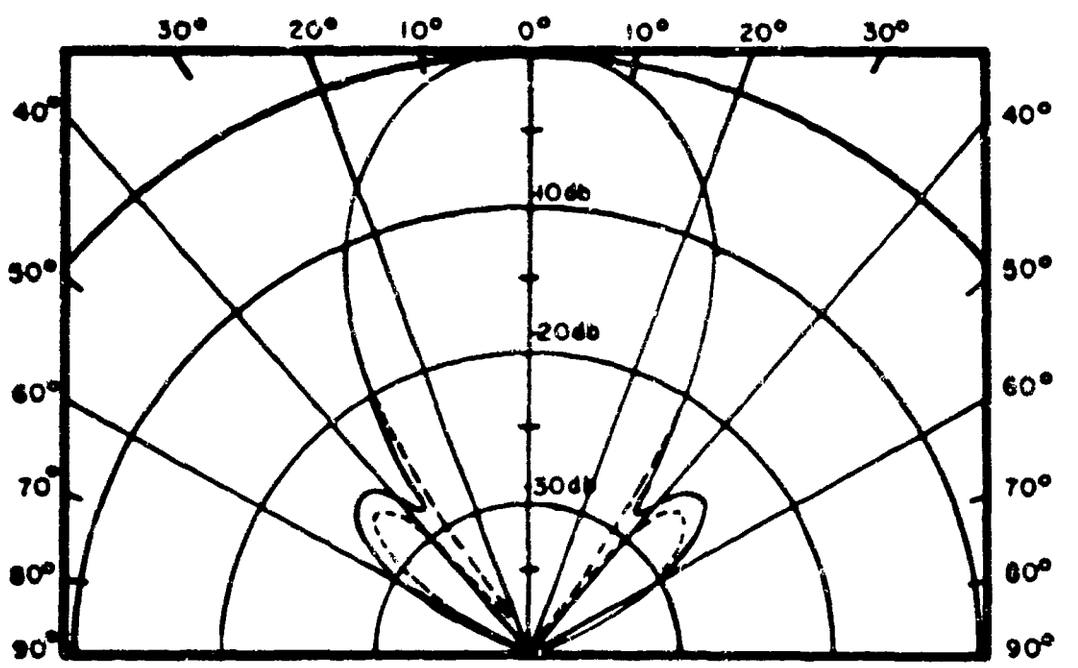

ℓ = 0, f = 9 KMC, NO PLASMA

——— EXPTL. DATA

-----THEORY (REF. 2, n = .426)

FIGURE 17 - H plane radiation patterns of the antenna shown in Fig. 9 at 9 KMC (rods in the Y direction).

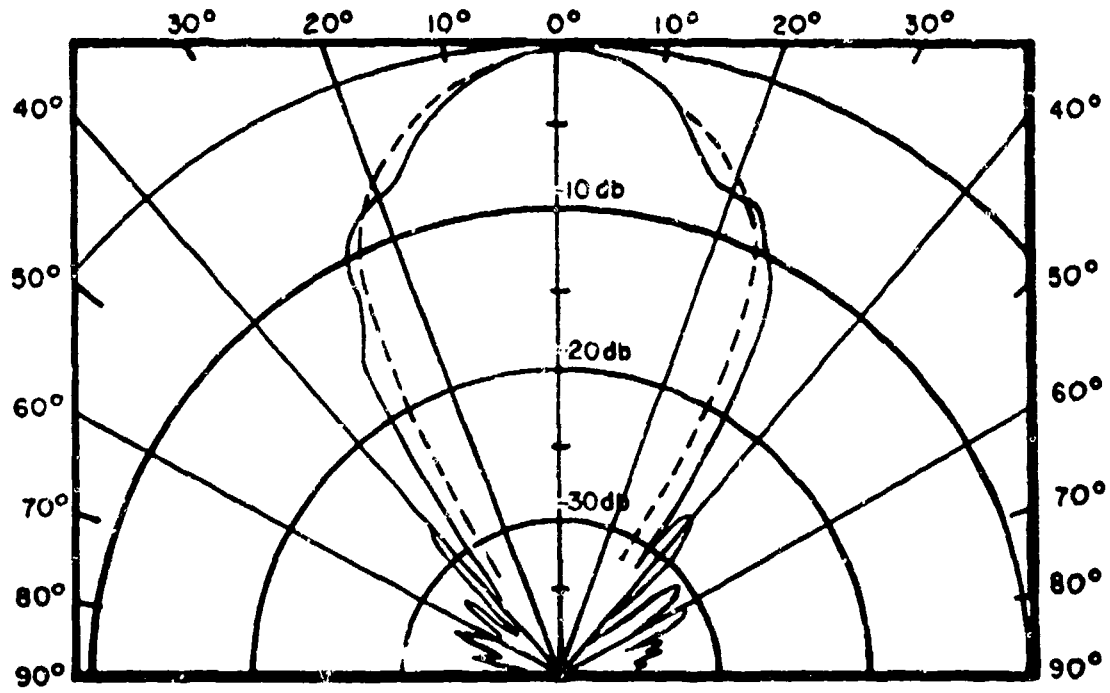

ℓ = 1.5", f = 10KMC, f_p = 8.1KMC

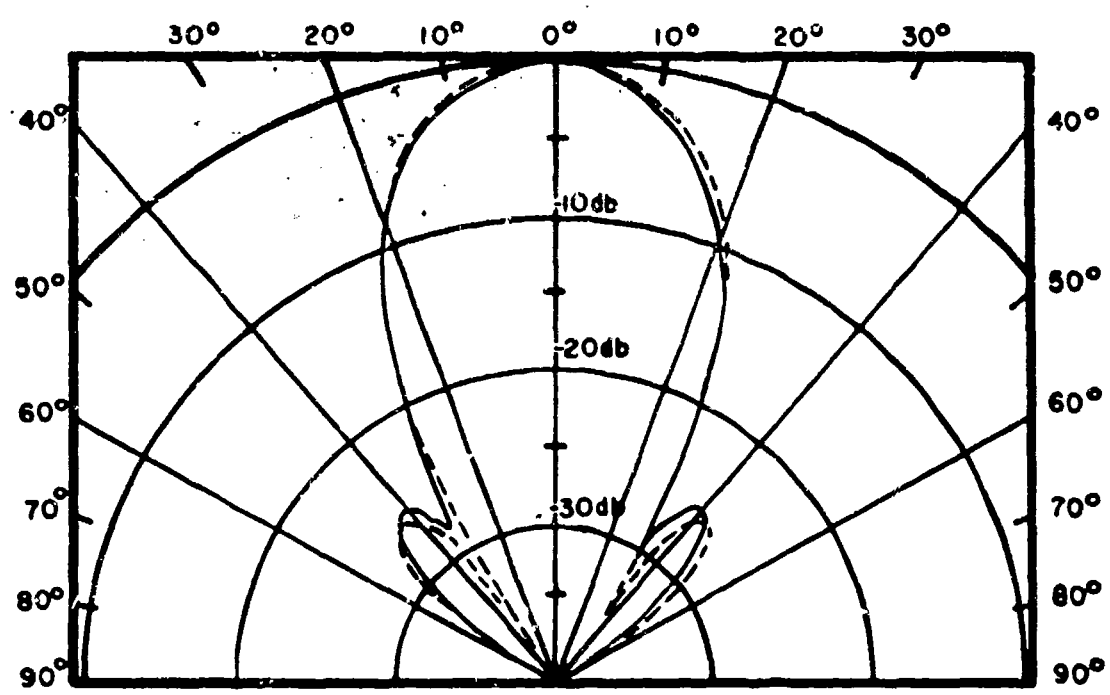

ℓ = 0, f = 10 KMC, NO PLASMA

——— EXPTL. DATA

---- THEORY (REF. 2, n = .564)

FIGURE 18 - H plane radiation patterns of the antenna shown in Fig. 9 at 10 KMC (rods in the Y direction).

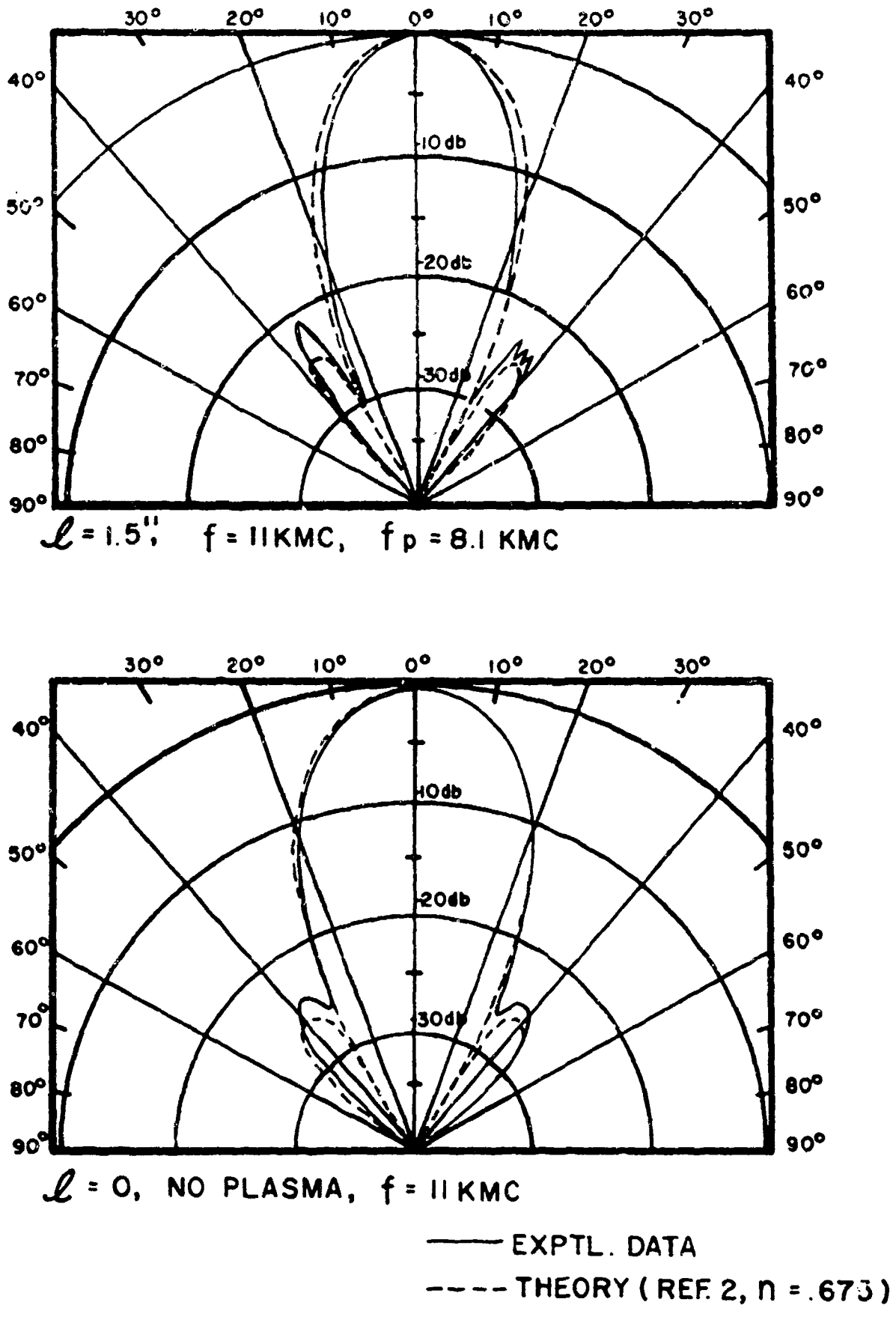

FIGURE 19 - H plane radiation patterns of the antenna shown in Fig. 9 at 11 KMC (rods in the Y direction).

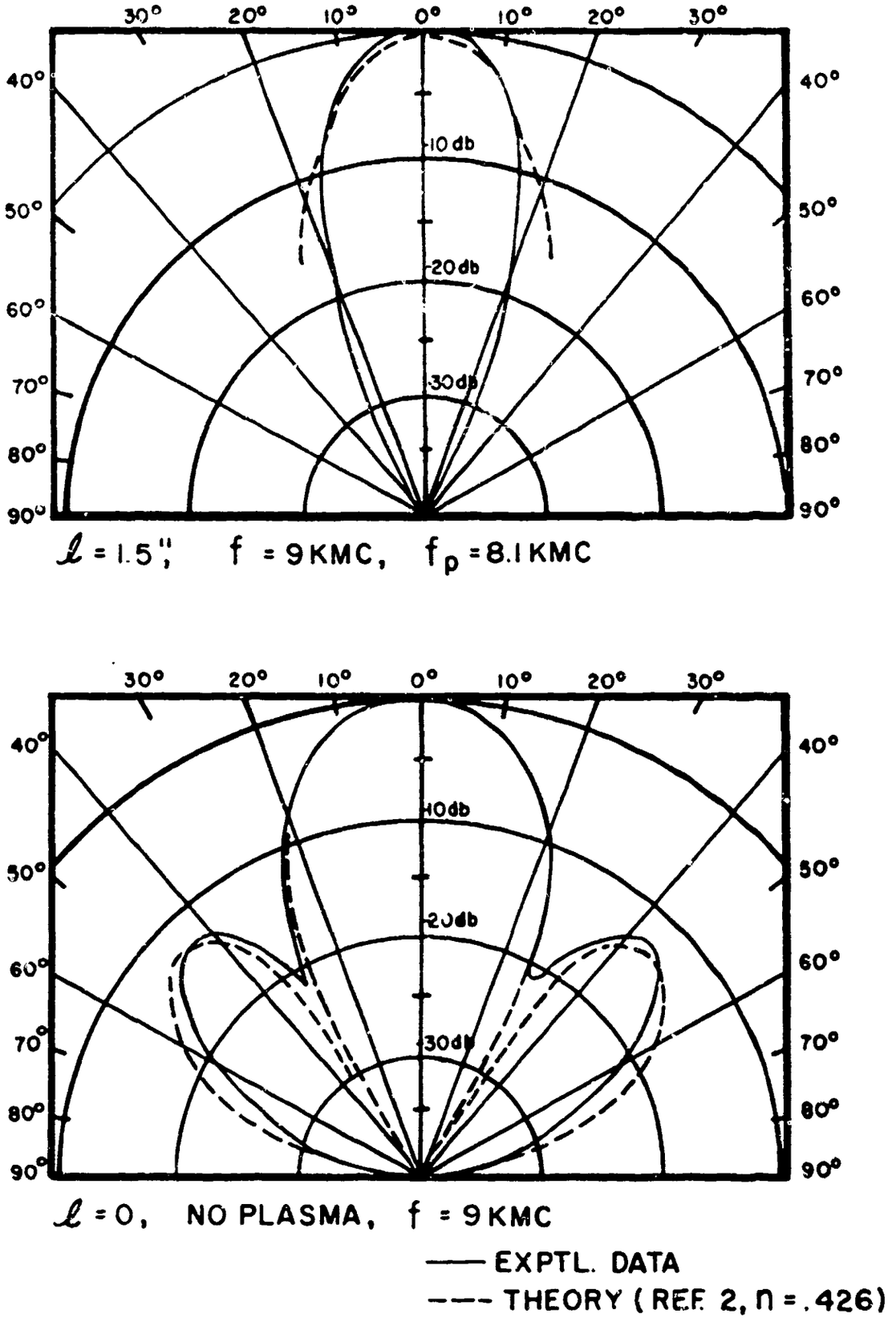

FIGURE 20 - E plane radiation patterns of the antenna shown in Fig. 9 at 9 KMC (rods in the Y direction).

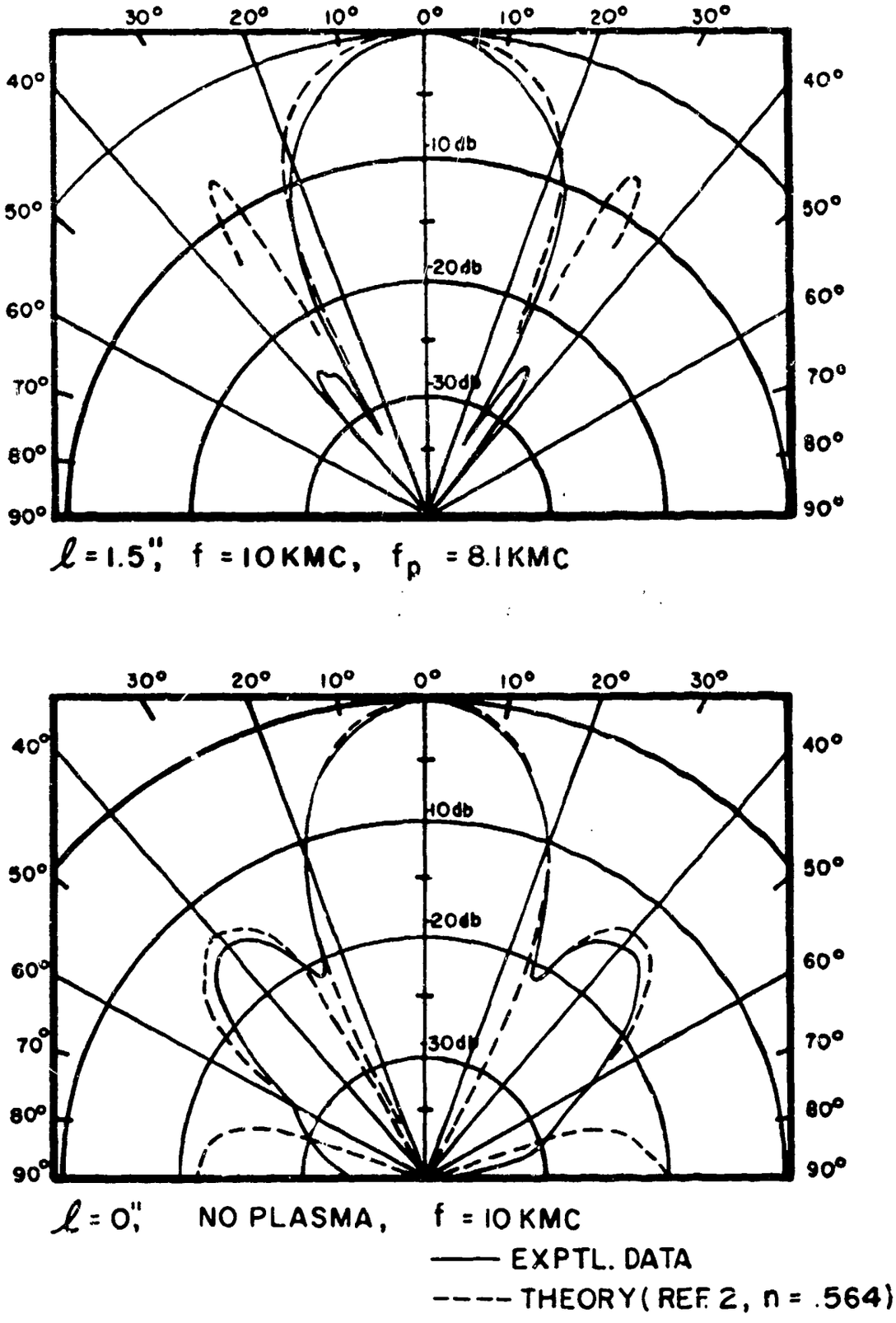

FIGURE 21 - E plane radiation patterns of the antenna shown in Fig 9 at 10 KMC (rods in the Y direction).

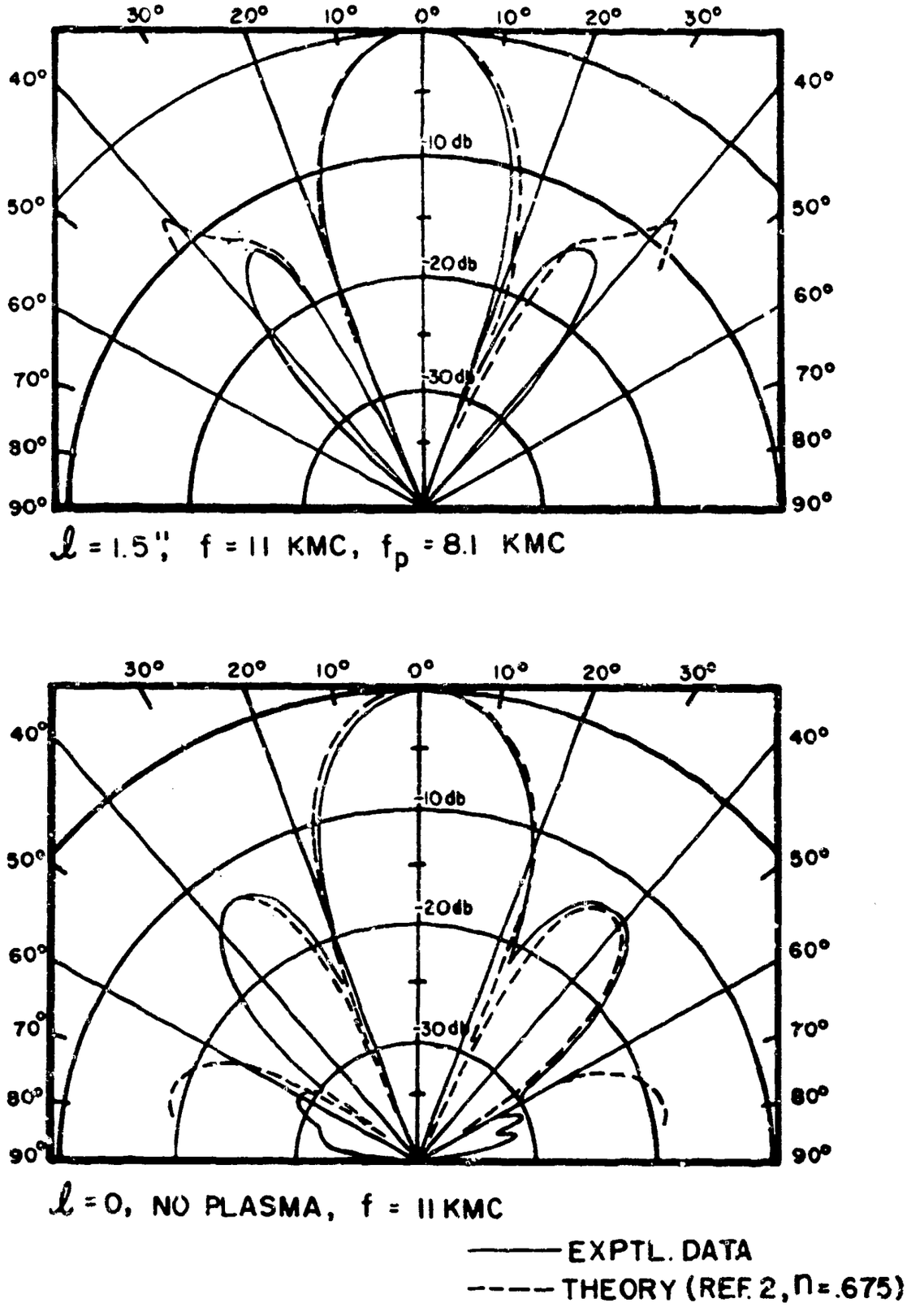

FIGURE 22 - E plane radiation patterns of the antenna shown in Fig. 9 at 11 KMC (rods in the Y direction).

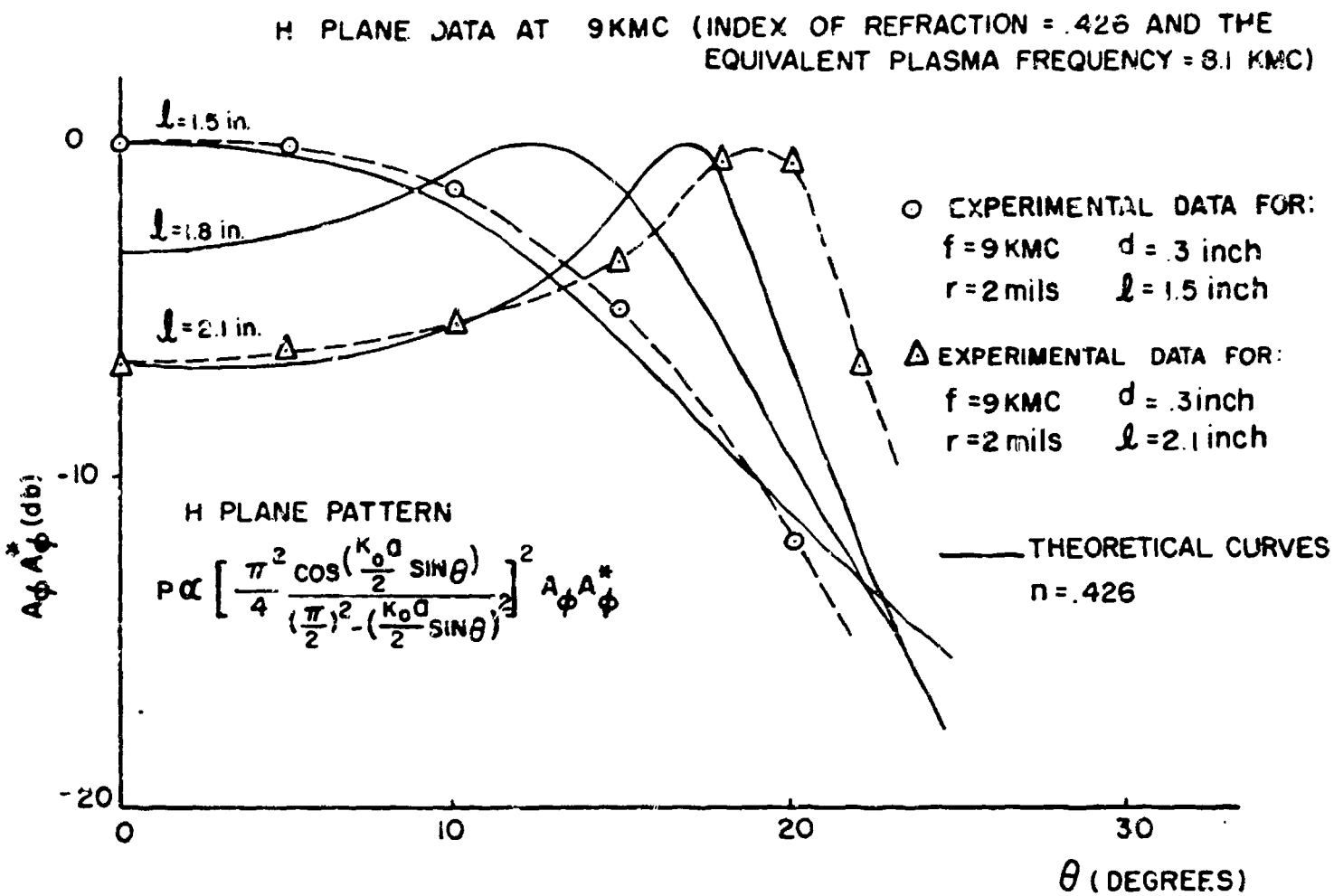

FIGURE 23 - Measured values of $A_\phi A_\phi^*$ at 9 KMC.

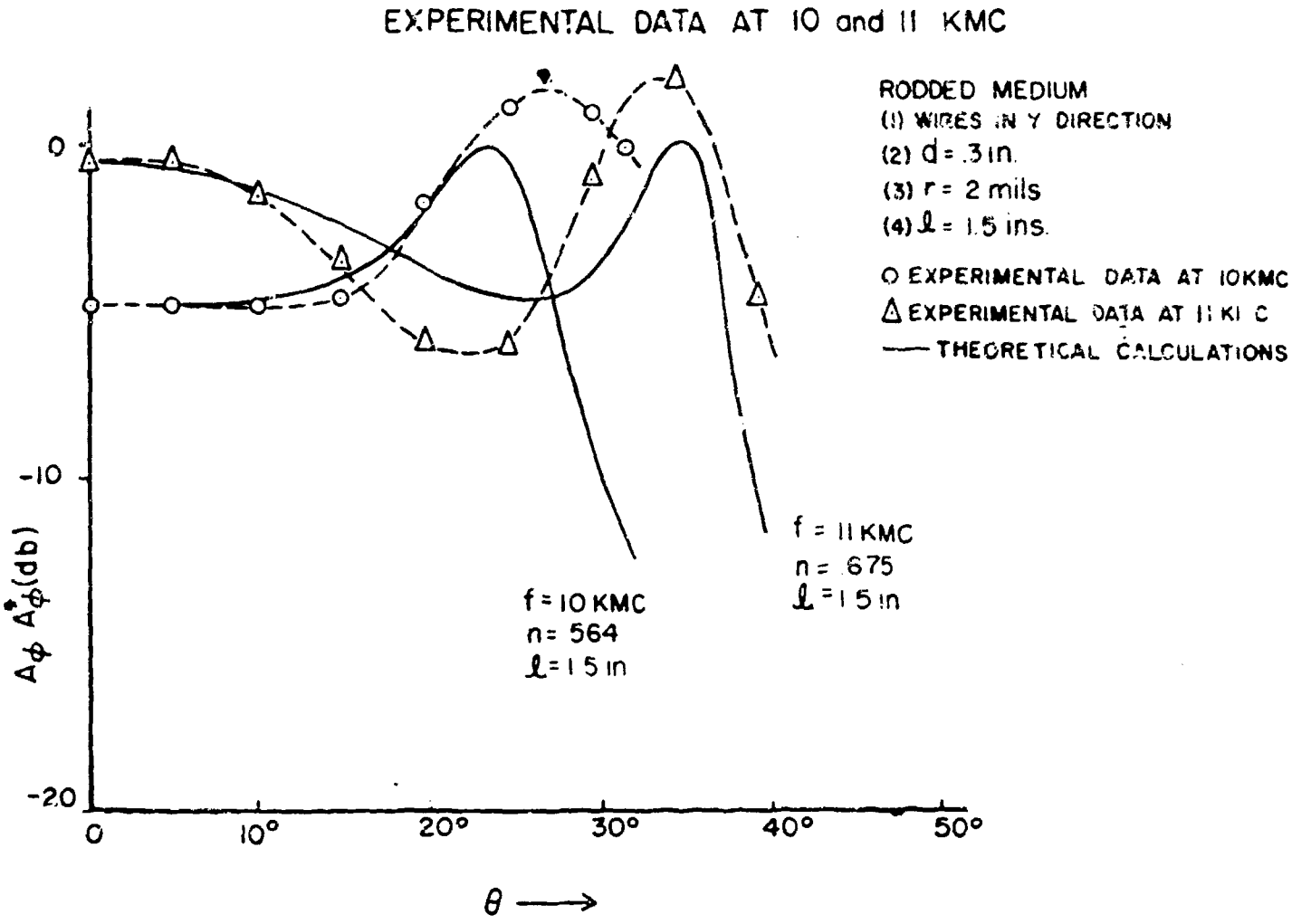

FIGURE 24 - Measured values of $A_\phi A_\phi^*$ at 10 and 11 KMC.

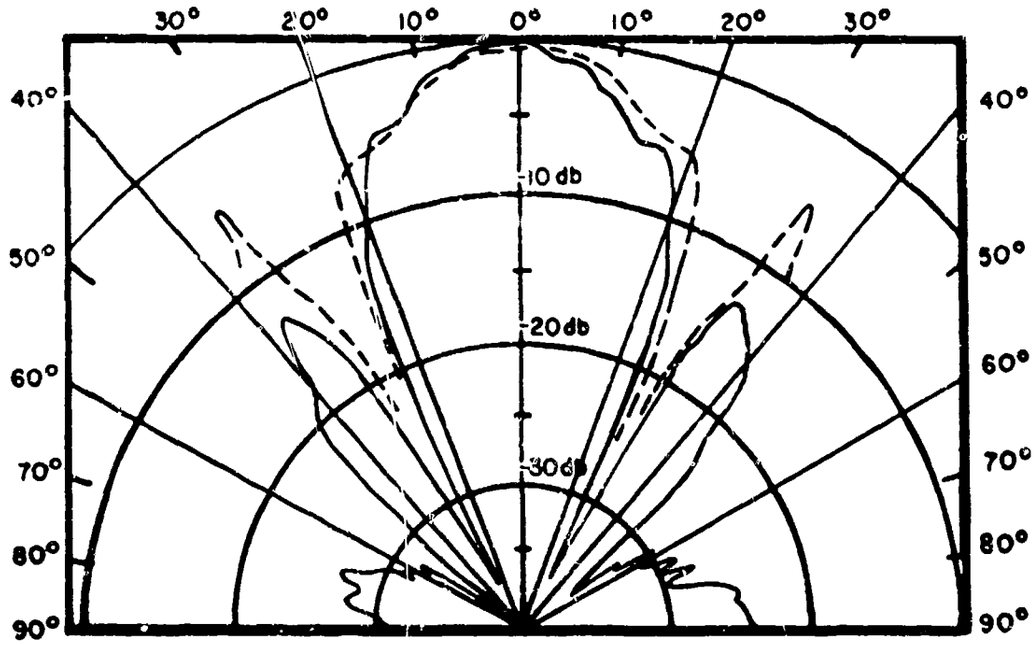

ℓ = 2.7", f = 10 KMC, f_p = 8.1 KMC

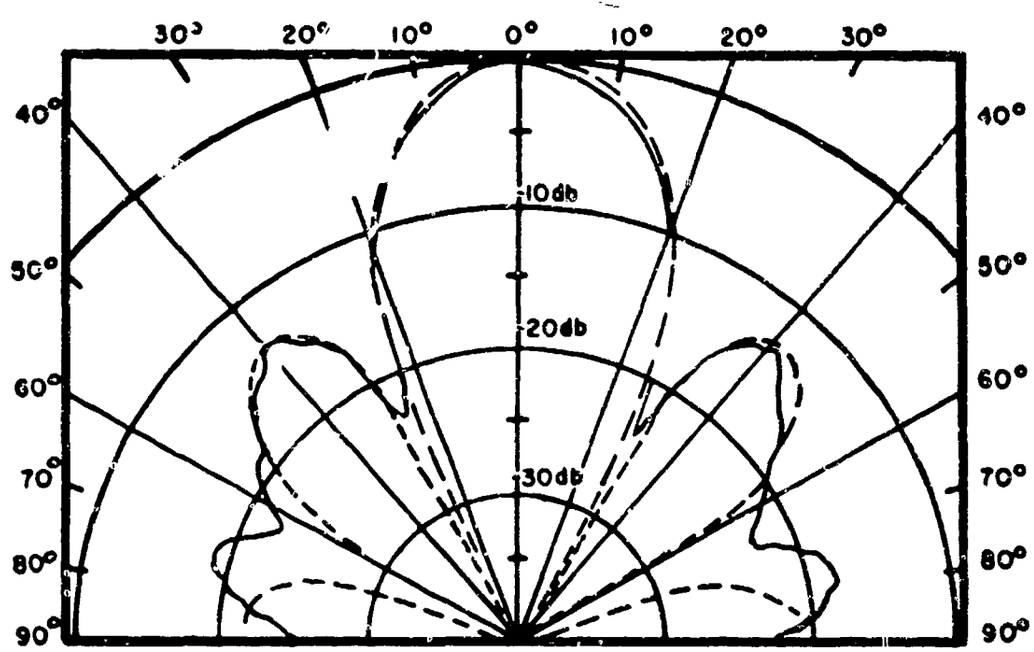

ℓ = 0, NO PLASMA, f = 10 KMC

——— EXPTL. DATA

- - - - THEORY (REF. 2, n = .564)

FIGURE 25 - E plane radiation patterns of the antenna shown in Fig. 12 at 10 KMC (rods in both the Y and Z directions).

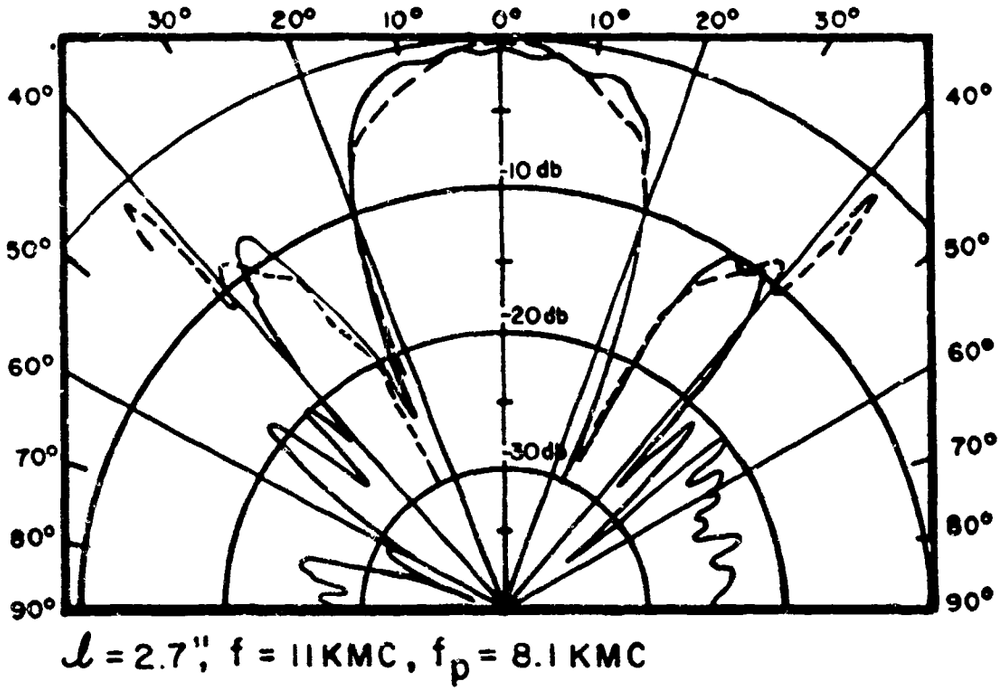

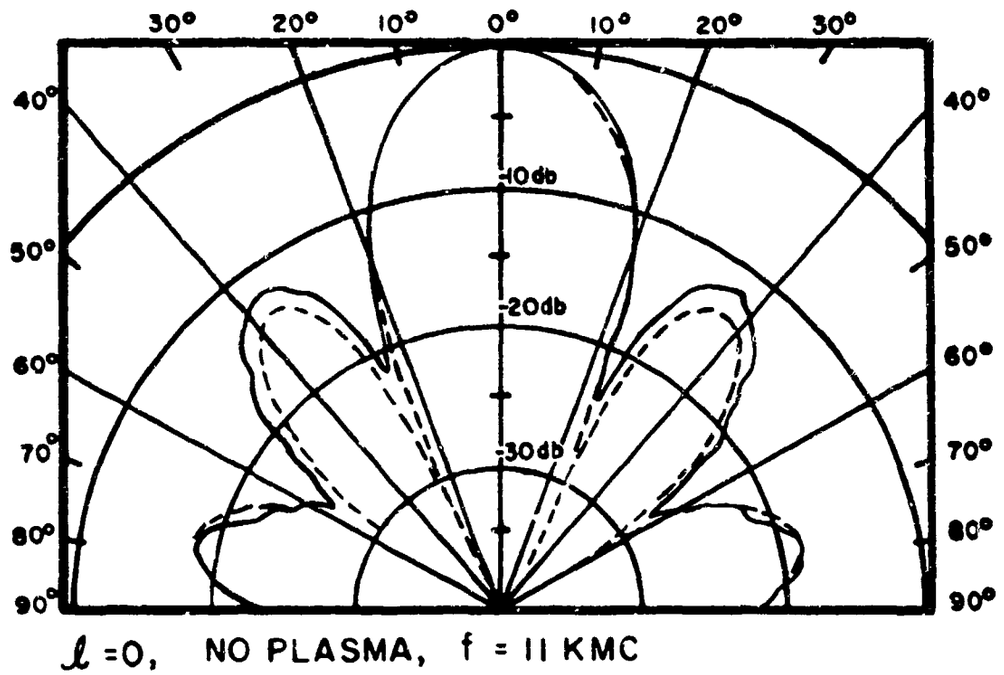

——— EXPTL. DATA

— — — THEORY (REF. 2, n=.675)

FIGURE 26 - E plane radiation patterns of the antenna shown in Fig. 12 at 11 KMC (rods in both the Y and Z directions).

Discussion of Experimental Results

The correlation between the H plane measurements and the theoretical calculations given by Equation (2) is very good, as seen from Figures 23 and 24. However, the agreement between the E plane measurements and the theoretical computations is less satisfactory. The sharp peaks in the radiation pattern occurring near the critical angle θ_c

$$\sin \theta_c = n,$$

predicted by Equation (1), were not observed in the E plane measurements. These sharp resonance phenomena require the correct phase relationships between all the radiating sources, and any deviation from this coherent phase relationship will tend to destroy the resonance. The lack of agreement between theory and experiment is partly attributable to the differences between the theoretical and experimental geometries. The experimental measurements are performed with a horn antenna and a simulated plasma slab of finite size, while the theoretical model is based on an infinite slot antenna and an unbounded plasma layer. The rodded medium also exhibits anisotropic behavior, and relative rod spacings d/λ_o used in these experiments are approaching an upper limit where the artificial dielectric starts to deviate from the behavior of a simple dielectric material. Aside from the lack of agreement around the critical angle θ_c, the radiation patterns are predicted reasonably well by Omura's[2] analysis.

The addition of the wires in the Z direction seems to improve the agreement between the measured and computed patterns to some extent, but the very sharp resonance is still not observed (see Figures 21, 22, 25 and 26.)

Since the physical geometries of the two rodded media are somewhat different, a quantitative statement about the improvements observed by adding the set of wires perpendicular to the ground plane is not warranted. The antenna geometry used with the rodded medium having rods in the Y direction only is shown in Figure 9, and the antenna geometry used with the artificial dielectric having rods in both the Y and Z directions is shown in Figure 12. In one case there were plastic rods and absorbing material present, and in the other case only the horn, ground plane, and rodded medium were present. In addition, one of the simulated slabs had a thickness of 1.5 inches while the other had a thickness of 2.7 inches. Further experimental investigations are needed in this area to gain a better understanding of the behavior of the different rodded media configurations.

In general, the radiation from the horn and simulated plasma sheath exhibits a rapid attenuation at angles greater than the critical angle θ_c, and the functions $A_\theta A_\theta^*$ and $A_\phi A_\phi^*$ have a maximum occuring at an angle slightly smaller than θ_c. The net result is that the radiation patterns may be drastically modified by the presence of a plasma layer, as illustrated in Figures 16 and 17.

Flock[3,4] predicted that the radiation pattern would have a secondary maximum due to the radiating sources in the plasma, but the position of the maximum is in disagreement with the experimental measurements because of the assumptions used in the theoretical model. Better correlation would be expected if more realistic current distributions in the plasma layer were employed in the analysis.

IV. CONCLUSIONS

This study has shown that the tensor permittivity of a homogeneous plasma in an infinite D.C. magnetic field can be simulated by a rodded medium. The rods in the artificial dielectric simulate the effects produced by the motions of the electrons in the plasma. Under the influence of an infinite magnetostatic field, the electrons in the plasma are constrained to move along the magnetic lines of force; similarly, the currents induced in the rodded medium are constrained to flow in the metallic wires thereby simulating the effects produced by the free electrons in the plasma. Waveguide measurements confirmed the anisotropic behavior of the rodded medium when the rods are oriented in one direction only.

The pattern experiments further substantiate the isotropic behavior of the rodded medium in a free space geometry. The antenna pattern measurements agree reasonably well with the theoretical model given in Reference 2, and demonstrate the effects a plasma sheath can exert on an antenna system. The pattern distortion observed in this experiment illustrates another important characteristic of plasma sheath transmission in addition to the more fully studied attenuation effects.

With reference to the horn geometry, it was shown that the simulation of the homogeneous isotropic properties of a plasma sheath could be achieved by a rodded medium which has wires oriented in both the Y and Z directions. It was further observed that the omission of wires in the Z direction altered the E plane pattern in the neighborhood of the critical angle θ_c and had little effect on the H plane patterns.

V. RECOMMENDATIONS FOR FUTURE RESEARCH

More experimental studies on the anisotropic behavior of the different rodded media configurations are needed. It has been shown, from a theoretical standpoint, that a rodded medium could simulate the anisotropic properties of a cold plasma in an infinite magnetostatic field, but a definitive experimental study would indicate to what degree the simulation is taking place. Experimental studies in the areas of eliminating re-entry blackout by applying a large D.C. magnetic field[29,30,31], the magnetic window effect, could be demonstrated using an anisotropic rodded medium with the rods oriented in one direction.

The addition of a loss mechanism to the artificial dielectric should also be investigated with the objective of developing techniques to simulate both the plasma and collisional frequencies in a free space geometry. The lossy artificial dielectric could be used to simulate more realistic plasma sheaths in laboratory antenna studies.

Collisional effects can be added to the rodded medium by employing lossy wires. Rotman[6] showed that the propagation constant of a rodded medium using lossy rods could be expressed as

$$\cosh \gamma d = \cos k_o d + j \frac{Z_o}{2Z_s} \sin k_o d$$

where

$\gamma = \alpha + j\beta =$ complex propagation constant of the rodded medium

$$\frac{Z_s}{Z_o} = \frac{R_o}{Z_o} + j \frac{d}{\lambda_o} \ln \left(\frac{d}{2\pi r} \right) .$$

The electric field is assumed to be parallel with the rods and R_s is the internal surface resistance of one of the equivalent wire grating structures. The surface resistance is equal to

$$R_s = d\,R_o$$

where R_o is the resistance per unit length of one of the rods. Ni-chrome wire can be utilized in the construction of a lossy rodded medium, but the equivalent collisional frequency is small. Larger and more realistic collision frequencies can be obtained by using rods which are constructed out of glass or dielectric fibers and are coated with a thin metallic film[32]. The resistance per unit length, R_o, of the dielectric coated rods can be of the order of hundreds of ohms per inch instead of the low values obtainable with the Ni-chrome wire.

Plasma simulation could also prove to be useful in microwave diagnostic studies of laboratory plasmas. The determination of some of the experimental limitations of a microwave diagnostic geometry (such as the errors introduced by the finite experimental geometry) could be obtained by replacing the actual laboratory plasma by a rodded medium.

A more practical application of the anisotropic characteristics of a rodded medium is the construction of a transmission type polarizer which converts a plane polarized wave into an elliptically polarized wave[33]. If the rods are oriented at 45° to the incident electric field of a plane wave and the parameters of the slab are chosen correctly, the emerging wave will be circularly polarized. This type of wave filter in optics is commonly called a "quarter-wave plate." The development of a quarter-wave plate which would convert a linear polarized antenna into a circularly polarized antenna could prove to be extremely useful.

REFERENCES

1. Tamir, T. and A. A. Oliner, "The influence of complex waves on the radiation field of a slot-excited plasma layer," IRE Trans. PGAP, vol. AP-10, pp. 55-65, January, 1962.

2. Omura, M., "Radiation pattern of a slit in a ground plane covered by a plasma layer," Air Force Cambridge Research Laboratory, AFCRL-62-958, December, 1962.

3. Flock, W. L., Plasma effects on microwave radiation, Ph.D. dissertation, Dept. of Engineering, University of California, Los Angeles, June, 1960.

4. Flock, W. L. and R. S. Elliott, "The radiation pattern of a microwave horn and a plasma layer," IRE Trans. PGAP, vol. AP-10, pp. 65-88, January, 1962.

5. Clayton, L. and J. S. Hollis, "Calculation of microwave antenna radiation systems by the Fourier integral method," Microwave Journal, vol. 3, no. 9, pp. 59-66, September, 1960.

6. Rotman, W., "Plasma simulation by artificial dielectric and parallel-plate media," IRE Trans. PGAP, vol. AP-10, pp. 82-95, January, 1962.

7. Collin, R. E., "A simple artificial anisotropic dielectric medium," IRE Trans. PGMTT, vol. MTT-6, pp. 206-209, April, 1958.

8. Kirschbaum, H. S. and S. Chen, "A method of producing broadband circular polarization employing an anisotropic dielectric," IRE Trans. PGMTT, vol. MTT-5, pp. 199-203, July, 1957.

9. Estrin, G., "The effects of anisotropy in a three dimensional array of conducting disks," Proc. IRE, vol. 39, pp. 821-826, July, 1951.

10. Delcroix, J. L., Introduction to the theory of ionized gases, Interscience Publishers, New York, 1960, pp. 67-73.

11. Elliott, R. S., "The tensor permittivity of a weakly-ionized plasma," Microwave Journal, vol. 2, no. 3, pp. 47-50, March, 1959.

12. Whitmer, R. F., "Principles of microwave interactions with ionized media," Microwave Journal, vol. 2, no. 3, pp. 47-50, March, 1959.

REFERENCES (Continued)

13. Brown, M. A., "Artificial dielectrics having refractive indices less than unity," Proc. IEE, Monograph no. 62R, vol. 100, part 4, pp. 51-62, May, 1953.

14. Brown, J. and W. Jackson, "The properties of artificial dielectrics at centimeter wavelengths," Proc. IEE, paper no. 1699R, vol. 102B, pp. 11-21, January, 1955.

15. Cohn, S. B., "Analysis of the metal strip delay structure for microwave lenses," J. Appl. Phys., vol. 20, pp. 257-262, March, 1949.

16. Cohn, S. B., "Electrolytic-tank measurements for microwave metallic delay lens media," J. Appl. Phys., vol. 21, pp. 674-680, July, 1950.

17. Collin, R. E., Field theory of guided waves, McGraw-Hill, New York, 1960, chapt. 9.

18. Brown, J., "The design of metallic delay dielectrics," Proc. IEE, vol. 97, part 3, pp. 45-48, January, 1950.

19. Macfarlane, G. G., "Surface impedance of an infinite parallel-wire grid at oblique angles of incidence," Journal IEE, vol. 93, part 3A, pp. 1523-1527, 1947.

20. Marcuvitz, N., Waveguide handbook, McGraw-Hill, New York, 1951, p. 285.

21. Jasik, H., Antenna engineering handbook, McGraw-Hill, New York, 1961, chapt. 14, p. 23.

22. Kittle, C., Introduction to solid state physics, Wiley, New York, 1956, pp. 162-163.

23. Von Hipple, A., Dielectrics and waves, Wiley, New York, 1954, pp. 97-98.

24. Moon, P. and D. E. Spencer, Foundations of electrodynamics, Van Nostrand Co., Princeton, N. J., 1960, p. 199.

25. Montgomery, C. G., Technique of microwave measurements, McGraw-Hill, New York, 1947, pp. 565-566.

26. Harrington, R. F., Time-harmonic electromagnetic fields, McGraw-Hill, 1961, p. 67.

27. Kock, W. E., "Metallic delay lenses," Bell Systems Technical Journal, vol. 27, pp. 58-82, January, 1948.

28. Silver, S., Microwave antenna theory and design, McGraw-Hill, New York, 1949, pp. 48-49.

29. Dirsa, E. F., "The telemetry and communication problems of re-entrant space vehicles," Proc. IRE, vol. 48, pp. 703-713, April, 1960.

30. Hodara, H., "The use of magnetic fields in the elimination of the re-entry blackout," Proc. IRE, vol. 49, pp. 1825-1830, December, 1961.

31. Hodara, H. and G. I. Cohn, "Radiation characteristics of a slot antenna in the presence of a lossy anisotropic plasma sheath," Proc. of the National Electronics Conference, Chicago, Ill., October 1961, vol. 17, pp. 622-631.

32. Golden, K. E. and T. M. Smith, "Simulation of a thin plasma sheath by a plane of wires," To be published in IEEE Transactions on Nucl. Sci., vol. NS-11, no. 1, January, 1964.

33. Ploussios, G., "A circular polarizer for linear polarized antennas," Paper presented at the Northeast Electronics Research and Engineering Meeting, Boston, Mass., November 4-6, 1963.

34. Jackson, J. D., Classical electrodynamics, Wiley, New York, 1962, p. 233.

35. Stone, J. M., Radiation and optics, McGraw-Hill, New York, 1963, chapt. 17.

36. Koerber, G. G., Properties of solids, Prentice-Hall, Englewood Cliffs, N. J., 1962, chapt. 7.

37. Stratton, J. A., Electromagnetic theory, McGraw-Hill, New York, 1941, p. 66.

APPENDIX A

Plane Wave Propagation in Anisotropic Dielectric

Plane wave type of propagation in an anisotropic dielectric,[34,35] will be discussed in this section. The propagation characteristics for a monochromatic wave with a time dependence given by $e^{+j\omega t}$ are obtained from Maxwell's Equations .

$$\bar{\nabla} \times \bar{E} = - j\omega\mu_o \bar{H} \tag{1a}$$

$$\bar{\nabla} \times \bar{H} = j\omega \bar{D} \tag{2a}$$

$$\bar{D} = \varepsilon_o [\varepsilon_r] [\bar{E}] \tag{3a}$$

Assuming the tensor $|\varepsilon_r|$ to be diagonalized with the coordinate axes oriented along the principal directions of the dielectric, Equation (3a) becomes

$$D_1 = \varepsilon_o \varepsilon_{11} E_1 \tag{4a}$$

$$D_2 = \varepsilon_o \varepsilon_{22} E_2 \tag{5a}$$

$$D_3 = \varepsilon_o \varepsilon_{33} E_3 \ . \tag{6a}$$

Taking the curl of Equation (1a)

$$\bar{\nabla} \times \bar{\nabla} \times \bar{E} = - j\omega\mu_o \bar{\nabla} \times \bar{H} \tag{7a}$$

and replacing $\bar{\nabla} \times \bar{H}$ with $j\omega\bar{D}$ yields the equation governing the propagation characteristics of the medium.

$$\bar{\nabla} \times \bar{\nabla} \times \bar{E} - k_o^2 [\varepsilon_r] [\bar{E}] = 0 \tag{8a}$$

If the propagation of the form $e^{-j\bar{k}\cdot\bar{r}}$ is assumed, the curl of the curl of the electric field can be replaced by

$$\bar{\nabla} \times \bar{\nabla} \times \bar{E} = - \bar{k} \times \bar{k} \times \bar{E} \ . \tag{9a}$$

Let the vector wavenumber $\bar{k}$ be represented by

$$\bar{k} = k\bar{n} \ , \tag{10a}$$

where $\bar{n}$ is a unit vector in the direction of $\bar{k}$. The substitution of Equations (9a) and (10a) into Equation (8a) yields the following expression:

$$\bar{n} \times \bar{n} \times \bar{E} + k_o^2/k^2 \ [\varepsilon_r] \ [\bar{E}] = 0 \tag{11a}$$

The vector identity

$$\bar{n} \times \bar{n} \times \bar{E} = (\bar{n}\cdot\bar{E}) \ \bar{n} - \bar{E} \tag{12a}$$

is used to simplify Equation (11a).

$$(\bar{n}\cdot\bar{E}) \ \bar{n} - \bar{E} + k_o^2/k^2 \ [\varepsilon_r] \ [\bar{E}] = 0 \tag{13a}$$

The rectangular components of Equation (13a) are

$$\left(k_o^2/k^2 \ \varepsilon_{11} + n_1^2 - 1\right) \ E_1 + n_2 \ n_1 \ E_2 + n_3 \ n_1 \ E_3 = 0 \tag{14a}$$

$$n_1 \ n_2 \ E_1 + \left(k_o^2/k^2 \ \varepsilon_{22} + n_2^2 - 1\right) \ E_2 + n_3 \ n_2 \ E_3 = 0 \tag{15a}$$

$$n_1 \ n_3 \ E_1 + n_2 \ n_3 \ E_2 + \left(k_o^2/k^2 \ \varepsilon_{33} + n_3^2 - 1\right) E_3 = 0 \tag{16a}$$

where k_o is the free space wavenumber and n_1, n_2, n_3 are respectively the X_1, X_2, and X_3 components of the unit vector $\bar{n}$. The solutions for k^2 are obtained by setting the determinant of the above set of homogeneous equations equal to zero.

In general, there are two modes of propagation described by Equations (14a), (15a) and (16a). One mode has a Poynting vector which is not parallel with the direction of the wave motion, and the other mode has a Poynting vector and vector wave number in the same direction. Table (1a) summarizes the values of k^2 for different polarizations and different directions of propagation.

TABLE 1a

Polarization of the Electric Field	Direction of Propagation	Propagation Constant
X_1 Axis	X_2 X_3 Plane	$k^2 = k_o^2 \ \varepsilon_{11}$
X_2 Axis	X_1 X_3 Plane	$k^2 = k_o^2 \ \varepsilon_{22}$
X_3 Axis	X_1 X_2 Plane	$k^2 = k_o^2 \ \varepsilon_{33}$
X_1 X_2 Plane	X_1 X_2 Plane	$k^2 = k_o^2 \left[\dfrac{\varepsilon_{11} \ \varepsilon_{22}}{n_1^2 \ \varepsilon_{11} + n_2^2 \ \varepsilon_{22}} \right]$
X_1 X_3 Plane	X_1 X_3 Plane	$k^2 = k_o^2 \left[\dfrac{\varepsilon_{11} \ \varepsilon_{33}}{n_1^2 \ \varepsilon_{11} + n_3^2 \ \varepsilon_{33}} \right]$
X_2 X_3 Plane	X_2 X_3 Plane	$k^2 = k_o^2 \left[\dfrac{\varepsilon_{22} \ \varepsilon_{33}}{n_2^2 \ \varepsilon_{22} + n_3^2 \ \varepsilon_{33}} \right]$

APPENDIX B

Certain restrictions are placed on the components of the tensor permittivity of the rodded medium because of the symmetries of the structure. In general, the tensor permittivity of an anisotropic material is expressed by

$$\begin{bmatrix} D_1 \\ D_2 \\ D_3 \end{bmatrix} = \begin{bmatrix} \varepsilon_{11} & \varepsilon_{12} & \varepsilon_{13} \\ \varepsilon_{21} & \varepsilon_{22} & \varepsilon_{23} \\ \varepsilon_{31} & \varepsilon_{32} & \varepsilon_{33} \end{bmatrix} \begin{bmatrix} E_1 \\ E_2 \\ E_3 \end{bmatrix} \tag{1b}$$

The constraints are obtained[36] by applying Neumann's principle when a symmetry operation is performed. In other words, the components ε_{ij} remain invariant under a coordinate transformation which corresponds to a symmetry operation.

The rodded medium under discussion in this section has all the rods oriented in the X_3 direction forming an infinite array of conducting cylinders throughout all space. The following symmetry operations can be imposed on the rodded medium because of the structural symmetries shown in Figure 2.

(1) 180 degree rotation about the X_1 axis.
(2) 180 degree rotation about the X_2 axis.
(3) 90 degree rotation about the X_3 axis.

Let the unprimed quantities be referred to the original coordinate system and the primed quantities be referred to the transformed coordinate system. The coordinate transformation can be expressed by

$$\begin{bmatrix} X_1' \\ X_2' \\ X_3' \end{bmatrix} = \begin{bmatrix} a_{11} & a_{12} & a_{13} \\ a_{21} & a_{22} & a_{23} \\ a_{31} & a_{32} & a_{33} \end{bmatrix} \begin{bmatrix} X_1 \\ X_2 \\ X_3 \end{bmatrix} \tag{2b}$$

The components of $[\varepsilon]$ in the primed coordinate system are given by[37]

$$\varepsilon'_{mn} = \sum_{i=1}^{3} \sum_{j=1}^{3} a_{mi} \; a_{nj} \; \varepsilon_{ij} \tag{3b}$$

where a_{mi} and a_{nj} are the components of the transformation matrix [A] shown in Equation (2b). The transformation matrix for a 180 degree rotation about the X_1 axis is equal to

$$[A] = \begin{bmatrix} 1 & 0 & 0 \\ 0 & -1 & 0 \\ 0 & 0 & -1 \end{bmatrix} \tag{4b}$$

The components ε_{ij} of the tensor permittivity obtained from Equation (3b) are listed below.

$$\varepsilon'_{11} = \varepsilon_{11}$$
$$\varepsilon'_{12} = -\varepsilon_{12}$$
$$\varepsilon'_{13} = -\varepsilon_{13}$$
$$\varepsilon'_{21} = -\varepsilon_{21}$$
$$\varepsilon'_{22} = \varepsilon_{22}$$
$$\varepsilon'_{23} = \varepsilon_{23}$$
$$\varepsilon'_{31} = -\varepsilon_{31}$$
$$\varepsilon'_{32} = \varepsilon_{32}$$
$$\varepsilon'_{33} = \varepsilon_{33}$$

The application of Neumann's principle

$$\varepsilon'_{ij} = \varepsilon_{ij}$$

yields the following allowable components of the tensor permittivity.

$$[\varepsilon] = \varepsilon_o \begin{bmatrix} \varepsilon_{11} & 0 & 0 \\ 0 & \varepsilon_{22} & \varepsilon_{23} \\ 0 & \varepsilon_{32} & \varepsilon_{33} \end{bmatrix} \tag{5b}$$

The transformation matrix for the 180 degree rotation about X_2 is given by

$$[A] = \begin{bmatrix} -1 & 0 & 0 \\ 0 & 1 & 0 \\ 0 & 0 & -1 \end{bmatrix} \tag{6b}$$

and allowable components of $[\varepsilon]$ under this symmetry operation are

$$[\varepsilon] = \varepsilon_o \begin{bmatrix} \varepsilon_{11} & 0 & \varepsilon_{13} \\ 0 & \varepsilon_{22} & 0 \\ \varepsilon_{31} & 0 & \varepsilon_{33} \end{bmatrix} \tag{7b}$$

The third symmetry operation, a 90 degree rotation about the X_3 axis, is given by the transformation matrix

$$[A] = \begin{bmatrix} 0 & 1 & 0 \\ -1 & 0 & 0 \\ 0 & 0 & 1 \end{bmatrix} \tag{8b}$$

and imposes the following constraints on the values of ε_{ij}.

$$[\varepsilon] = \begin{bmatrix} \varepsilon_{11} & \varepsilon_{12} & \varepsilon_{13} \\ -\varepsilon_{12} & \varepsilon_{11} & \varepsilon_{13} \\ \varepsilon_{31} & \varepsilon_{31} & \varepsilon_{33} \end{bmatrix} \tag{9b}$$

Since Equations (5b), (7b) and (9b) must be satisfied simultaneously, the following components are zero.

$$\begin{aligned} \varepsilon_{12} &= 0 \\ \varepsilon_{13} &= 0 \\ \varepsilon_{21} &= 0 \\ \varepsilon_{23} &= 0 \\ \varepsilon_{31} &= 0 \\ \varepsilon_{32} &= 0 \end{aligned}$$

Therefore, the resulting tensor permittivity of the rodded medium illustrated in Figure 2 is equal to

$$[\varepsilon] = \varepsilon_o \begin{bmatrix} \varepsilon_{11} & 0 & 0 \\ 0 & \varepsilon_{11} & 0 \\ 0 & 0 & \varepsilon_{33} \end{bmatrix} \tag{10b}$$